Title: Using multi-modal neuroimaging to characterise social brain specialisation in infants

Authors: Maheen Siddiqui[1*], Paola Pinti[1], Sabrina Brigadoi[2,3], Sarah Lloyd-Fox[4], Clare E. Elwell[5], Mark H. Johnson[4], Ilias Tachtsidis[5†], Emily J.H. Jones[1*†]

Affiliations:
[1]Centre for Brain and Cognitive Development, Birkbeck College, University of London, UK
[2]Department of Development and Social Psychology, University of Padova, Italy
[3]Department of Information Engineering, University of Padova, Italy
[4]Department of Psychology, University of Cambridge, UK
[5]Department of Medical Physics and Biomedical Engineering, University College London, UK

***Correspondence:**
Joint corresponding authors
m.siddiqui@bbk.ac.uk
e.jones@bbk.ac.uk

†Joint last authorship

Abstract

The specialised regional functionality of the mature human cortex partly emerges through experience-dependent specialisation during early development. Our existing understanding of functional specialisation in the infant brain is based on evidence from unitary imaging modalities and has thus focused on isolated estimates of spatial or temporal selectivity of neural or haemodynamic activation, giving an incomplete picture. We speculate that functional specialisation will be underpinned by better coordinated haemodynamic and metabolic changes in a broadly orchestrated physiological response. To enable researchers to track this process through development, we develop new tools that allow the simultaneous measurement of coordinated neural activity (EEG), metabolic rate and oxygenated blood supply (broadband near-infrared spectroscopy) in the awake infant. In 4-to-7-month-old infants, we use these new tools to show that social processing is accompanied by spatially and temporally specific increases in coupled activation in the temporal-parietal junction, a core hub region of the adult social brain. During non-social processing coupled activation decreased in the same region, indicating specificity to social processing. Coupling was strongest with high frequency brain activity (beta and gamma), consistent with the greater energetic requirements and more localised action of high frequency brain activity. The development of simultaneous multi-modal neural measures will enable future researchers to open new vistas in understanding functional specialisation of the brain.

Introduction

The adult brain is highly specialised, with core networks coordinating to subserve complex behaviours. This specialised functioning emerges across development through a combination of genetically influenced brain architecture and experience-expectant learning processes (generalised neural development that occurs as a result of common experiences) and experience-dependent (variation in the environment contributing to individual differences in neural response) [1]. During early development, infants undergo significant neural, physiological, and socio-cognitive changes that are accompanied by large-scale changes in social communication and interaction. Currently, we have relatively few tools that allow us to comprehensively capture the emergence of functional specialisation in the infant social brain. Developing new approaches is critical for advancing our understanding of early brain physiology and cognitive function.

Identifying appropriate metrics to index functional specialisation in the infant brain should be informed by theoretical perspectives on how functional specialisation develops. Interactive specialisation is a theory of brain development that posits that functional specialisation emerges through competition between brain regions [2]. Thus, functional specialisation can be indexed as a smaller spatial extent of neural responses to a particular stimulus category and concomitant selectivity in responsive regions [3]. Typically, the extent and selectivity of brain activation is measured through indirect indices of oxygenated blood flow (e.g. functional near-infrared spectroscopy or fNIRS [4] or functional magnetic resonance imaging or fMRI [5]) or of coordinated neural activity (e.g. electroencephalography or EEG [6]). However, one mechanism that may contribute to competition between brain regions is the limited energetic resources available to the infant brain. The brain is an energetically costly organ, consuming 20-25% of the body's energy in adulthood while representing only 2% of the body's mass [7], [8]. There are also substantial developmental changes in the brain's energy consumption; in the first year of life, up to 60% of available energy is used by the brain [9]**.** When brain regions become functionally active (for example during stimulus processing) neurons fire more rapidly, requiring greater supplies of adenosine triphosphate or ATP (energy stores). Producing ATP requires oxygen, and this is supplied through a localised increase in oxygenated haemoglobin in the blood. Increases in oxygenated haemoglobin do not happen concurrently in all brain areas, and there are spatial dependencies between activated and deactivated regions in the adult brain [10]. Energy supplies are important to synaptic plasticity, memory and learning [11], and the mechanism through which energy supplies are coupled to activation (neurovascular coupling) also develops through experience-dependent specialisation in the infant brain [12]. Thus, energy supply constraints may be one factor that contributes to the emergence of brain specialisation. If this is the case, detecting functional specialisation in infancy requires not only examining measures of neural activity and oxygenated haemoglobin, but also identifying whether particular regions show stronger coupling between neuronal demand and energetic supply.

As a first step, testing such frameworks requires the availability of methods that can measure the spatial extent and stimulus selectivity of neuroenergetics coupling in infancy. Previous studies have typically used single modalities sensitive to distinct aspects of brain function. For example, studies with fMRI indicate that core regions of the social brain (particular the fusiform face area) show increases in oxygenated haemoglobin delivery in response to faces by 4-9 months [13]. Further, functional near-infrared spectroscopy (fNIRS) studies show that oxygenated haemoglobin delivery in response to naturalistic social videos in a broad region of temporal cortex emerges over the first hours of life [14]. Work with EEG indicates

developmental increases in differentiated theta power responses to social versus non-social stimuli between 6 and 12 months [3]. Thus, work with single modalities indicates development in functional specialisation across the first year of life.

Broadband near-infrared spectroscopy (or bNIRS) is a new technique that uses a broad range of optical wavelengths which allows the measurement of the oxidation state of mitochondrial respiratory chain enzyme cytochrome-c-oxidase (CCO), thereby providing a direct measure of cellular energy metabolism [4]. CCO is located in the inner mitochondrial membrane and serves as the terminal electron acceptor in the electron transport chain (ETC). It therefore accounts for 95% of cellular oxygen metabolism. In this way, bNIRS allows non-invasive measurement of cellular energy metabolism alongside haemodynamics/oxygenation in awake infants.

Work with single modalities has demonstrated that social selectivity in core regions of the adult 'social brain' can be robustly detected by 4 – 7 months of age, [15]–[18]. We recently showed the feasibility of using bNIRS in 4-to-7-month-old typically developing infants [19] and demonstrated the presence of unique task-relevant, regionally specific functional networks where high levels of haemodynamic and metabolic coupling were observed. Here, we integrate this methodology with EEG to examine whether specific brain regions show coordinated energetic coupling and neural activity. We develop a novel analysis pipeline to identify localised coupling responses that are modulated by naturalistic social content. We aimed specifically to investigate the relationship between low- and high-frequency neural activity with haemodynamics and metabolism. For EEG, we expected an increase in neural activity in response to the social condition and a decrease in neural activity in response to the non-social condition. Based on previous work, this was expected to be strongest in the theta frequency band [3]. Moreover, for the combined bNIRS-EEG analyses, we hypothesised differentiated haemodynamic/metabolic coupling with neural activity for the social and non-social stimulus conditions. We performed two types of statistical tests: a) individual comparisons of the social and non-social conditions and b) comparison of the social condition versus the non-social condition. The individual condition tests were performed to show the scale and spatial location/sensitivity of the coupling between haemodynamics/metabolism and neural activity for each condition. Meanwhile, the social versus non-social comparison was performed to show where there was a significant difference in the coupling between the two conditions. With comparison (a) we aimed to identify regions involved in the processing of social and non-social stimuli by identifying the regions where the coupling was significant. With comparison (b) we aimed to identify regions where coupling was significantly different between conditions. We predicted that for the individual comparison of the social condition, we would observe positive associations between bNIRS and EEG measures, i.e. a simultaneous increase in haemodynamics/metabolism and neural oscillatory activity in the beta and gamma frequency bands (based on previous combined EEG – fMRI studies [20]–[26]) which would be localised to core social brain regions. We hypothesised that for the non-social condition, over the same brain regions, positive associations would be observed between bNIRS and EEG measures, but they would be a simultaneous decrease in haemodynamics/metabolism and oscillatory activity. We also expected simultaneous increases in haemodynamics/metabolism and oscillatory activity to be localised to the parietal brain region. These predictions are based on our previous work [19] where we demonstrated that stronger coupling between haemodynamics and metabolism was observed in the temporo-parietal regions for the social condition and in parietal region for the non-social condition which is known to play an important role in object processing [27], [28]. For the social versus the non-social contrast, we predicted that haemodynamic activity and

metabolism would be coupled with neuronal oscillatory activity more strongly for the social stimuli in comparison to the non-social stimuli, with significant differences being observed in the temporo-parietal regions.

Results

Naturalistic social stimuli elicit expected increases in broadband EEG activity: 5-month-old infants n=42) viewed naturalistic social and non-social stimuli (Fig 1a) while we concurrently measured EEG and broadband NIRS. Fourier-transform of continuously recorded EEG data from 32 channels (n=35) in one-second segments across the time course of stimulus presentation confirmed robust broadband increases in neural activity in response to social versus non-social stimuli (Fig 1b, replicating [3]).

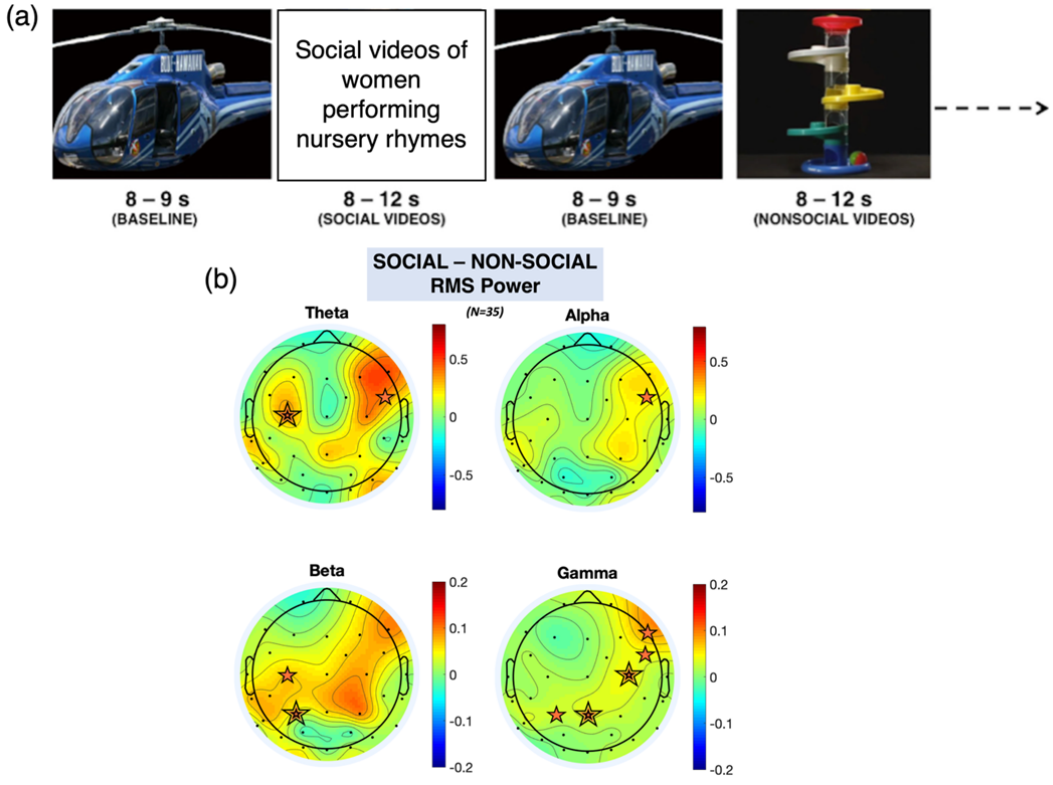

Figure 1: a) Illustration of the paradigm; b) Scalp topographies of the grand average RMS power for theta, alpha, beta, and gamma frequency bands (averaged across participants, averaged across the stimulus period) for the social minus non-social condition. The orange stars indicate statistically significant EEG electrodes where an increase in activity was observed (e.g., increase in response to the social condition compared to the non-social condition); a double line indicates significance after FDR correction.

Haemodynamic and metabolic coupling and oscillatory activity spatially overlap: We used a method that we have previously validated to integrate haemodynamic and metabolic signals from the bNIRS data (n=25) to investigate the relationship between the two signals [19], [29]. Using this method, we obtained indices that indicated whether specific brain regions either had a high level of coordinated coupling between haemodynamics and metabolism (i.e. coupled increases in metabolic function and oxygenated blood flow) or a

mismatched coupling (i.e. an increase metabolic function and a concurrent decrease in oxygenated blood flow). This revealed distinct locations sensitive to social (Fig 2b) and non-social (Fig 2d) processing; the topography of these locations is similar to the topography of differentiated broadband EEG activity (Fig 2a, c), particularly for haemodynamic and metabolic coupling at channels 12 and 14 and EEG theta band activity.

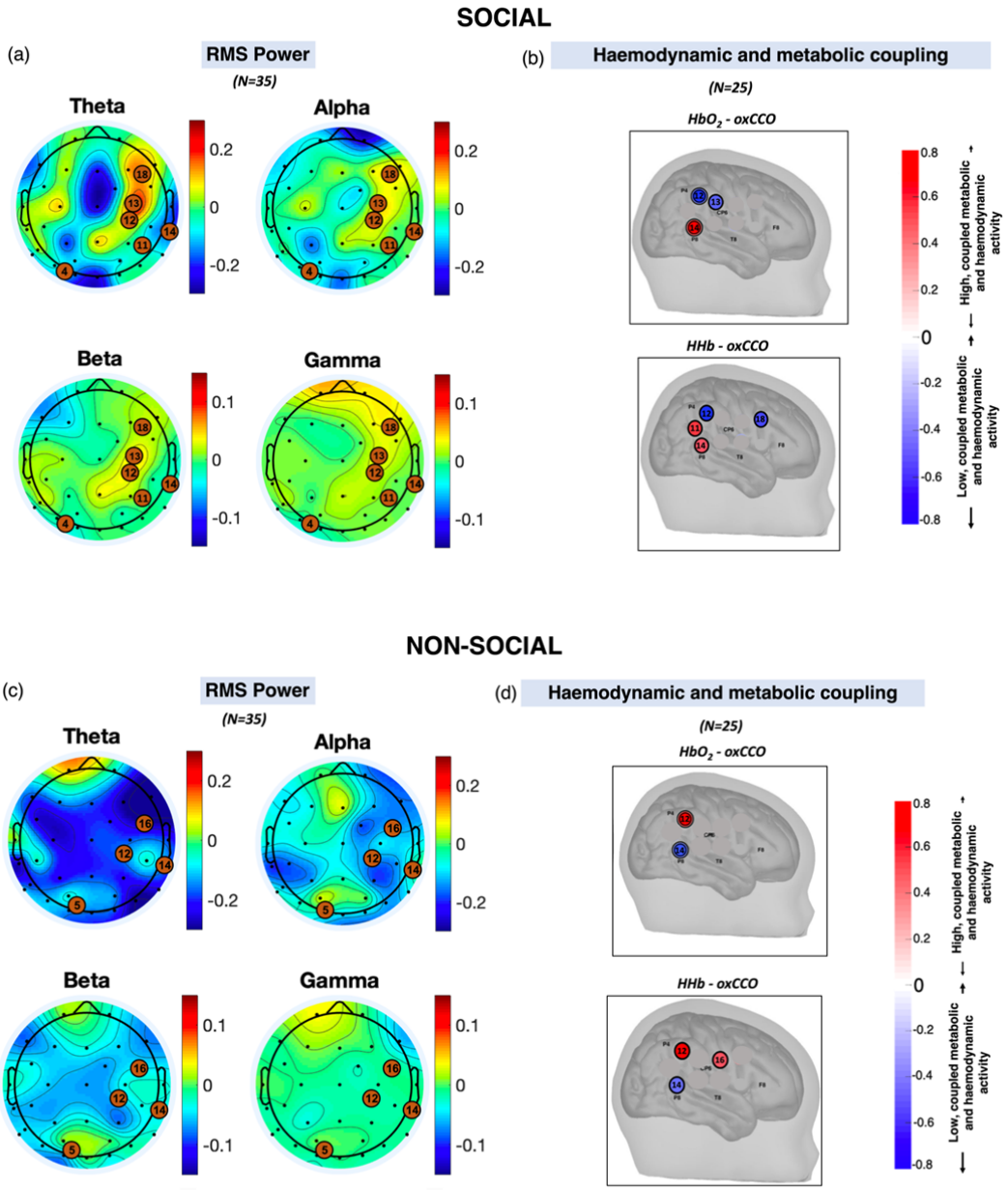

Figure 2: Scalp topographies of the grand average RMS power for theta, alpha, beta, and gamma frequency bands (averaged across participants, averaged across the stimulus period for (a) social and (c) non-social conditions. The black dots show the locations of the EEG electrodes while the orange circles represent the bNIRS channels. Locations of high haemodynamic and metabolic coupling for (b) social and (d) non-social condition. Figure 2b and 2dn are reproduced from Figure 7, Siddiqui et al. 2022.

Coupled signals highlight specialised activation in the temporal parietal junction: We then convolved the time-course of the block-averaged within-hemisphere EEG time-series responses with an infant-specific haemodynamic response function (n=14; Fig 3). A general

linear model (GLM) approach was then used to identify FDR-corrected associations between all EEG locations and the bNIRS channels that showed significant coupling between the metabolic and haemodynamic response (Fig 2b, d). In line with the results shown in Fig 2b and Fig 2d, we expected the spatial coupling between bNIRS and EEG to differ for the social and non-social conditions. We predicted that for the social condition, we would observe coordinated increases in haemodynamic/metabolic activity (HbO_2 and oxCCO) and neural oscillatory activity (positive associations between bNIRS and EEG) in the beta and gamma frequency bands over the temporo-parietal region. Meanwhile we expected that for the non-social condition, we would observe coordinated decreases in haemodynamic/metabolic (HbO_2 and oxCCO) activity and neural oscillatory activity (also resulting in positive associations between bNIRS and EEG) over the temporo-parietal region and coordinated increases over the parietal region. We expected negative associations between HHb and oxCCO for both conditions. We predicted that the comparison of social versus non-social would show associations between bNIRS and EEG was stronger for the social condition.

Figure 3 supplement 1 shows the individual statistical comparisons of the social (red colour scale) and non-social (blue colour scale) conditions. For both conditions, bNIRS – EEG coupling was consistently observed between bNIRS channel 14 and various EEG channels, which were positioned over the parietal and superior temporal sulcus – temporal parietal junction regions respectively. For the social condition, a coupled increase in haemodynamic/metabolic activity and neural oscillatory activity was observed in the beta, gamma, and high-gamma frequency bands, which was primarily concentrated in the temporo-parietal region (e.g., bNIRS channel 14 and EEG electrodes Pz, PO4). A consistent pattern of coupling with neuronal activity was observed across chromophores particularly for the beta band. For the non-social condition, no coupling was observed between haemodynamics and neural activity (i.e., HbO_2 and HHb) for the low-frequency theta and alpha frequency bands. Meanwhile, a coupled increase in metabolic activity and neural activity was observed between bNIRS channel 14 and occipital and parietal EEG locations (O2, PO8, P10, P4 for the theta band and P10 for the alpha band). Moreover, in the high-frequency beta, gamma and high-gamma bands, coupling was observed primarily for HHb and oxCCO between bNIRS channel 14 and occipital, and parietal EEG locations (Oz, O2 and PO8). A consistent pattern of coupling was observed between HHb and oxCCO. Several long-range associations were also observed such as those in the beta frequency bands between bNIRS channels 12 and 13 and EEG locations TP8 and T8 respectively for the social condition for HbO_2 and between bNIRS channel 14 and EEG locations C2 and Cz for the non-social condition for HHb and oxCCO.

Figure 3 supplement 2 shows the statistical comparison of the social versus the non-social condition. Not many significant differences were observed between bNIRS and EEG associations for the two conditions. Significant differences were observed between bNIRS channel 14 and Pz (with stronger association for the social condition) in the gamma frequency band for HbO_2. Meanwhile, significant differences were observed between bNIRS channel 14 and O2 (with stronger association for the non-social condition) in the high-gamma band for oxCCO. This suggests differential coupling between haemodynamic/metabolic activity and neural activity for each condition.

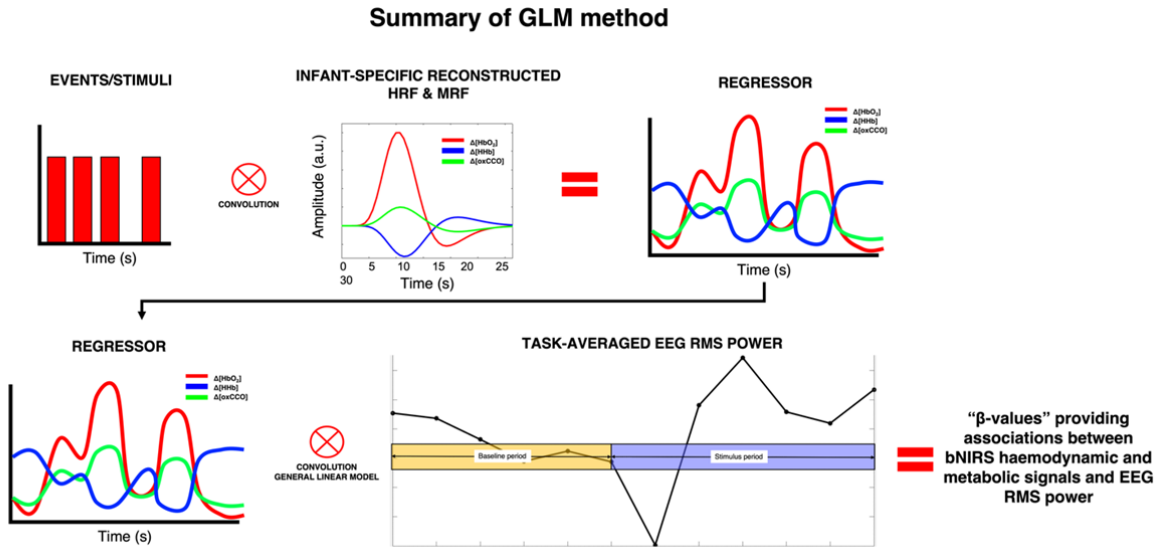

Figure 3: Summary of the procedure for obtaining the associations between bNIRS signals and EEG RMS power at each bNIRS combination, for each frequency band.

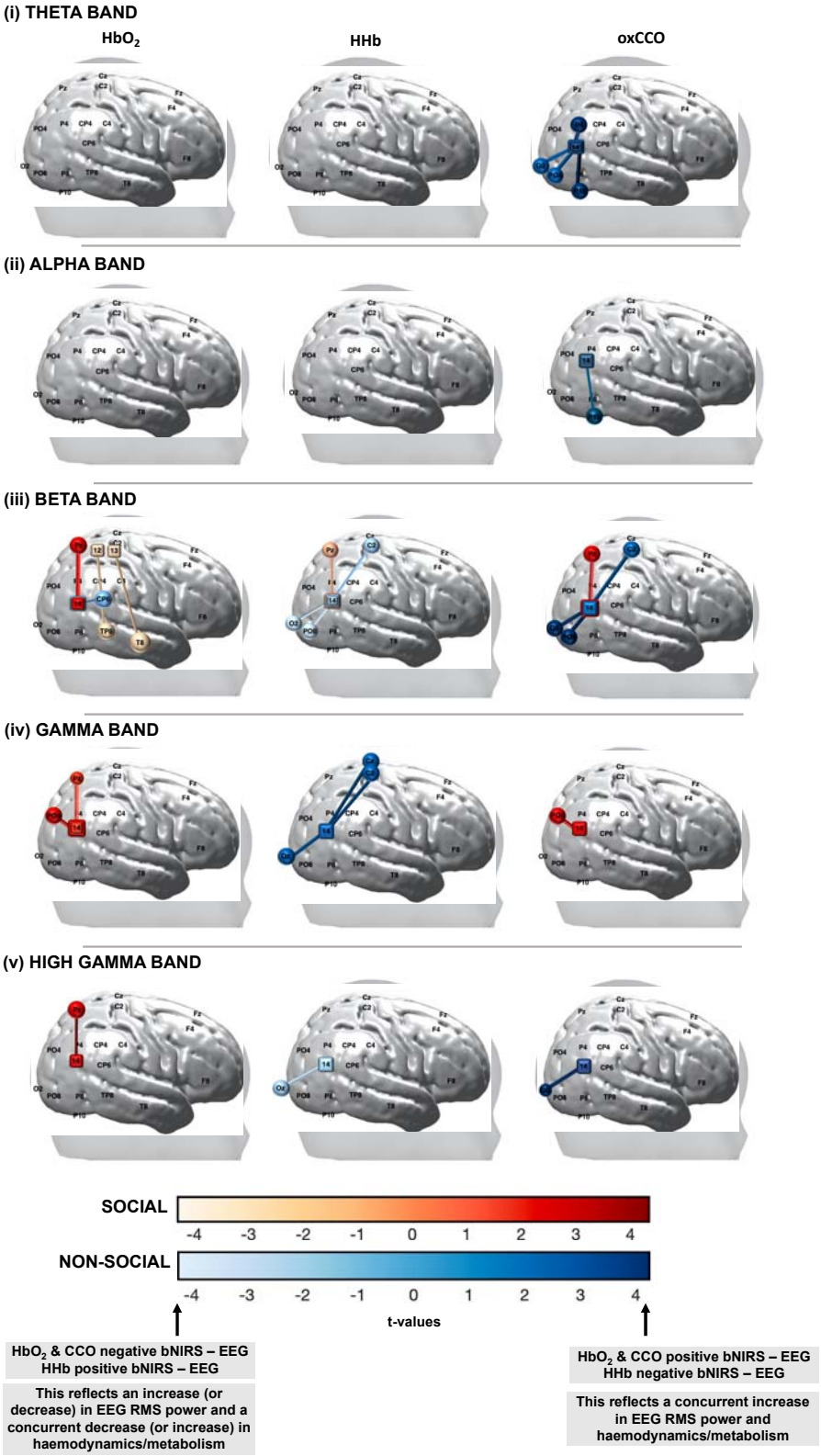

Figure 3 supplement 1: FDR-corrected significant connections between bNIRS channels (squares) and EEG electrodes (circles) for the (i) theta, (ii) alpha, (iii) beta, (iv) gamma and (v) high gamma bands for the social condition (red colour bar) and the non-social condition (blue colour bar) for HbO_2, HHb, and oxCCO.

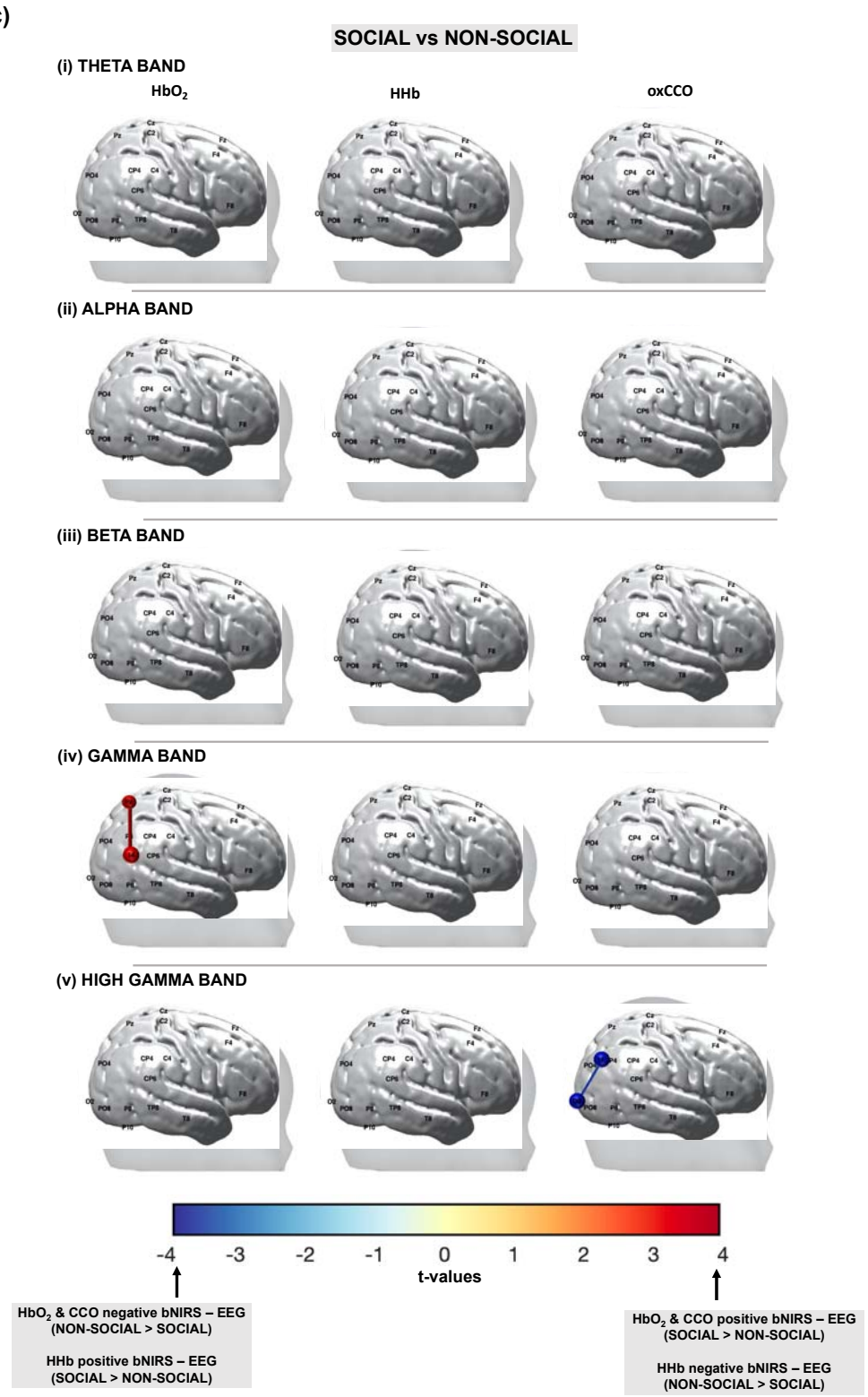

Figure 3 supplement 2: FDR-corrected significant connections between bNIRS channels and EEG electrodes for the (i) theta, (ii) alpha, (iii) beta, (iv) gamma and (v) high gamma bands for the social condition versus the non-social condition for HbO_2, HHb, and oxCCO. The colour bar represents the t-values from the GLM analysis with a positive t-value representing a significant, positive connection between the bNIRS channel and EEG electrode while a negative t-value represents a negative connection.

Using image reconstruction on the bNIRS data, the spatial sensitivity of the bNIRS location that showed the clearest differences in coupling (channel 14) are shown in Figure 4. The method for image reconstruction has been described in detail in the methods section. The results indicate that the bNIRS – EEG coupling was most consistent with the spatial extent changes in metabolic activity (CCO).

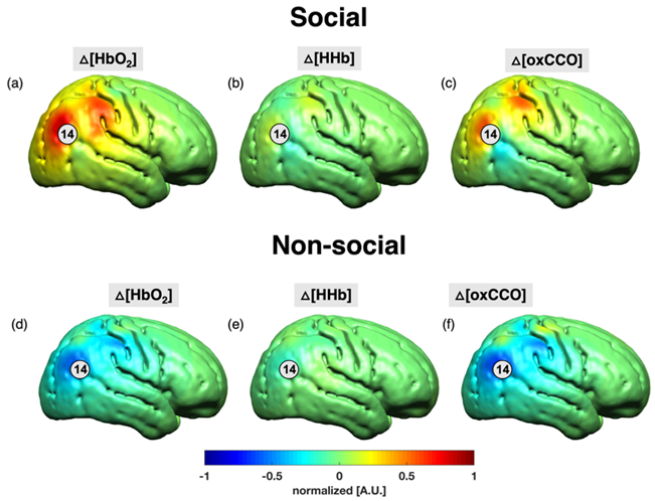

Figure 4: Grand-average image reconstruction at 18 s post-stimulus onset for the social condition (a – c) and the non-social condition (d – f) at a single time point of 18 s post-stimulus onset. The concentration changes for HbO_2 and HHb were normalised to the maximum concentration change of HbO_2 while ΔoxCCO was normalised to its own maximum change in concentration. Channel 14 has been indicated.

Discussion

We develop a tool that enabled multimodal imaging analysis of coordinated neural activation, metabolic demand, and oxygenated haemoglobin delivery in the infant brain. As a proof of principle, we examined the relationship between these measures to identify regional selectivity to social versus non-social stimuli. To first demonstrate the scale and spatial sensitivity of the coupling between haemodynamic/metabolic activity and neuronal oscillatory activity, comparisons were performed individually for the social and non-social conditions. For this, we predicted a simultaneous increase in haemodynamics/metabolism and neural activity in the beta and gamma frequency band. We predicted that for the social condition this would be localised to the core social brain regions (temporo-parietal region) while for the non-social condition, we expected the coupling to be localised to parietal regions, known to be involved in object processing [27], [28]. We additionally expected a simultaneous decrease in haemodynamic/metabolic activity and neural activity over the temporo-parietal region for the non-social condition, in accordance with our previous work [19]. Next, to demonstrate differential coupling for social and non-social stimuli, we performed a comparison of the social condition versus the non-social condition. For this, we hypothesised that in the beta and gamma frequency bands, there would be stronger coupling between haemodynamics/metabolism and neural activity for the social condition over the temporo-parietal region.

Confirming previous work, naturalistic social and non-social stimuli produce broad haemodynamic changes, with smaller spatial extent of locations with coupled haemodynamic and metabolic activity [19]. We also replicated previously observed greater EEG responses to

social versus non-social stimuli [3]. However, examining coupling between these two phenomena uncovered a precise pattern in which specific locations in the parietal and temporo-parietal regions showed differential coupling between bNIRS-EEG for social and non-social stimuli, particularly for the beta and gamma band frequency bands, as we predicted. We contend that this approach identifies a more localised regional area with selective coordination of neural, haemodynamic, and metabolic activity. The increased localisation observed in our coupling analysis may indicate our approach provides a more rigorous measure of functional specialisation. Widespread use of this technique will accelerate our understanding of both the typically and atypically developing brain. Unexpectedly, while most associations between haemodynamic/metabolic activity and oscillatory activity were localised, we observed several long-range connections between haemodynamic/metabolic and neural signals. It has been hypothesised that long-range functional connectivity patterns are vital for the organisation of human brain structure and function [30]. The strongest coupling was observed between temporo-parietal bNIRS channel 14 with parietal EEG locations Pz and PO4 for the social condition (for beta and gamma frequency bands). Meanwhile, for the non-social condition, coupling was observed between temporo-parietal bNIRS channel 14 with occipital and parietal EEG locations Oz, O2, PO8 and P10 (for theta and beta frequency bands). While an overall consistent pattern of associations across chromophores and conditions was observed, some variability was also seen, particularly across frequency bands. This was expected and in line with previous EEG-fMRI studies that have demonstrated task-dependent variation in coupling between neural and haemodynamic activity across frequency bands [20]–[26]. For example, for resting state simultaneous fMRI and EEG, stronger coupling between the BOLD response and neural activity has been observed for the alpha band [31]. Meanwhile, for cognitive tasks, stronger coupling has been observed in the gamma frequency band [32]. Scheeringa et al. [20] investigated trial-by-trial coupling of EEG and BOLD activity and found that low- and high-frequency bands independently contribute to explaining BOLD variance. We therefore expected the frequency band showing the strongest coupling between bNIRS and EEG for each of the stimuli to vary. Further, while we did expect and observe significant overlap in associations between chromophores within each frequency band, some variability was seen. For example, for the social condition, no associations were observed in the low-frequency bands for any of the chromophores. Moreover, in the beta frequency bands, all chromophores displayed significant associations between bNIRS channel 14 and Pz for the social condition and both HHb and oxCCO displayed significant associations between bNIRS channel 14 and O2, PO8 and C2. Similarly, in the gamma frequency bands, both HbO_2 and oxCCO displayed significant associations between bNIRS channel 14 and PO4. The variability that was observed between chromophores was limited mostly to the non-social condition. For example, only oxCCO displayed significant associations between bNIRS and EEG for the low-frequency theta and alpha frequency bands. It is well known that various components involved in neurovascular coupling undergo development postnatally, see the review by [33] for a full discussion. Briefly, there is extensive structural change within cerebral microvasculature including growth, extension and proliferation of new blood vessels [34], [35]. Further, studies have also demonstrated gradual development of vascular reactivity (i.e., change in vascular tone, vasoconstriction and vasodilation) [20], [21] which is necessary for the propagation of the NVC response [38]. Lastly, pericytes and astrocytes which are key components of NVC are also known to undergo development in size, number, connectivity and branching [12], [39]–[41]. From the metabolic perspective, infant positron emission tomography (PET) studies demonstrate regional-specific, progressive increase in the cerebral metabolic rate of oxygen consumption ($CMRO_2$) [42] while others evidence a developmental maturational change in oxidative metabolism [43]. In adults, previous research has also

suggested that oxygen consumption is more spatially localised in comparison to changes in cerebral blood flow [44] and that oxCCO has distinct spatial distributions in the brain [45], [46], [47], indicating that energy metabolism may be more spatially specific. The spatial distribution of oxCCO in different brain regions currently remains unmapped in the developing infant brain, however. Therefore, taken together, given that during early development there are extensive changes in cerebral vasculature as well as the metabolic environment and potential variability in the spatial distribution of oxCCO, it is expected that there will be some variability observed in the associations between the haemodynamics and metabolism with neural activity. In our study, we observed more consistent oxCCO – EEG associations across frequency bands and stimuli with more localised (fewer long-range) associations. Further studies with a larger sample size and longitudinal follow up can provide a clearer view on how NVC develops in infancy which will help explain some of the observed variability. Moreover, future studies with high density bNIRS arrays will provide clarification on the spatial distribution of oxCCO in the infant brain.

EEG profiles observed in the present study are consistent with previous studies in identifying increased gamma band activity over temporal and parieto-occipital brain regions during face processing [48]–[61]. High-frequency neural firing is associated with localised processing [62] whilst lower-frequency activity is associated with larger-scale network changes and transfer of information across systems [63]. The increase in lower-frequency activity during social attention also observed here and in other work [3], [64] may support larger-scale connectivity and communication of information through cross-frequency coupling [49]. Our work further indicates that measures of metabolic load may provide important additional information in understanding localisation of brain function. Localised high-frequency activity exerts strong metabolic demand [65], [66] and subsequent increases in oxygenated haemoglobin [25], [67], [68]. These increases in metabolic rate are supported by increased activity in the mitochondrial electron transport chain, resulting in the changes in cytochrome-c-oxidase we detected with broadband NIRS. Nitric oxide (which competes with oxygen to bind to cytochrome-c-oxidase) and carbon dioxide (produced as a by-product in the ETC) are key signalling molecule in controlling neurovascular coupling and thus subsequent oxygen delivery [69], [70]. Finally, reactive oxygen species produced by the ETC are a key signal in inducing synaptic plasticity [71]. Thus, our work is consistent with a model in which social attention induces localised high frequency brain activity in the temporal parietal junction, which increases local metabolic rates, triggering synaptic plasticity and subsequent oxygen delivery to a broader region.

Our work particularly highlights the temporal-parietal junction is showing strong coupling and social selectivity. Previous studies measuring haemodynamic activity have identified early sensitivity of this region to social stimuli from at least 4 months [72], alongside a broader network of other regions. Here, we pinpoint this specific location as having coupled neuronal, metabolic, and haemodynamic activity that is modulated in opposite directions by complex social and non-social content. In the adult brain, the temporal-parietal junction has received considerable attention and there are several competing models of its function. It has been linked to mentalising [73], [74] and reorienting attention to behaviourally relevant stimuli [75]; it can be viewed as a nexus area where the convergence of attention, language, memory and social processing supports a social context for behaviour ([76] or as a region that is active when awareness of a prediction permits attentional control [77]. Intriguingly, recent formulations within the predictive coding framework link the right temporal-parietal junction to a domain-general role in prediction, perhaps representing the precision of priors [78]. Predictability has been linked to energy-efficiency, with some computational models showing

that energy limitations are the only requirement for driving the emergence of predictive coding [79]. Increases in beta/gamma have also been linked to unexpected reward processing [80]. Taken together, our results may indicate the early presence of priors for social interaction that are being actively updated (in contrast to the dynamic toys, which may already be more predictable).

The methods we developed could be broadly applied to study both neurotypical and atypical brain function. Assessing coupling over developmental time may reveal the mechanisms underpinning neural specialisation and constrain theoretical frameworks seeking to explain specialisation in the adult brain. The mechanisms of neurovascular coupling remain unclear in the adult brain [69], and are developing in infancy [12], and novel multimodal and non-invasive approaches to their identification could yield significant progress. Computational models could test the role of constraints in energy supply on developing localisation of function. Further, the region identified here also shows atypical haemodynamic responsiveness in infants with later symptoms of autism [18]; since mitochondrial dysfunction has become an increasing focus in autism [81] the possibility that atypical coupling may impact specialisation in autism is an important hypothesis to test. Further, our methods have applicability in determining the impacts of early brain injury. Recent work [82] measured both cerebral oxygenation and energy metabolism in neonates with brain injury (hypoxic-ischaemic encephalopathy) and demonstrated that the relationship between metabolism and oxygenation was able to predict injury severity. This therefore provided a clinical, non-invasive biomarker of neonatal brain injury. Indicating applicability across the lifespan [83] simultaneous measurements of cerebral oxygenation, metabolism and neural activity in epilepsy revealed unique metabolic profiles for healthy brain regions in comparison to those with the regions of the epileptic focus. The work in epilepsy demonstrates the strength of combining measurements from multiple modalities to investigate brain states, particularly in clinical populations.

Our work has several limitations. We used naturalistic stimuli to maximise ecological validity; however, this reduces our ability to probe the function of the temporal-parietal junction across specific stimulus dimensions and this is an important target for future work. Limitations of current technology meant we recorded from the right hemisphere only and thus cannot determine the specificity of our findings to left temporal-parietal junction; engineering advances are required to produce whole-head bNIRS devices. Moreover, we only studied one age group of infants between 4 and 7 months therefore, we could not investigate developmental change.

Conclusion: Energy metabolism and neural activity are known to be tightly coupled in order to meet the high energetic demands of the brain, both during a task [84], [85] and at rest [86]. It has been hypothesised that the level of correspondence between energy metabolism and neuronal activity may be an indicator for brain specialisation [84], [87], [88]. Here, we developed a system to simultaneously measure multichannel broadband NIRS with EEG in 4-to-7-month-old infants to investigate the neurovascular and neurometabolic coupling. We presented a novel study combining bNIRS and EEG and show stimulus-dependent coupling between haemodynamic, metabolic, and neural activity in the temporal-parietal junction. The results highlight the importance of investigating the energetic basis of brain functional specialisation and opens a new avenue of research which may show high utility for studying neurodevelopmental disorders and in clinical populations where these basic mechanisms are altered.

Acknowledgements

M.F.S was funded by the BBSRC [BB/J014567/1], the Birkbeck Institutional Strategic Support Fund (ISSF) and the ESRC (ES/V012436/1). E.J.H.J was supported by the ESRC (ES/R009368/1). E.J.H.J, M.H.J. and M.F.S. were also supported by the AIMS-2-TRIALS programmes funded by the Innovative Medicines Initiative (IMI) Joint Undertaking Grant No. 777394. This Joint Undertaking receives support from the European Union's Horizon 2020 research and innovation programme, with in-kind contributions from the European Federation of Pharmaceutical Industries and Associations (EFPIA) companies and funding from Autism Speaks, Autistica and SFARI. I.T. was supported by the Wellcome Trust (104580/Z/14/Z). S.L.F was supported by a UKRI Future Leaders Fellowship (MR/S018425/1) and S.L.F and C.E.E received support from the Bill and Melinda Gates Foundation (OPP1127625). M.H.J and EJHJ received support from the UK Medical Research Council (MR/K021389/1 & MR/T003057/1) received support from the UK Medical Research Council (MR/K021389/1 & MR/T003057/1). S.B. was supported by the Progetto STARS Grants 2017 (C96C18001930005) from the University of Padova.

The work presented herein was conducted at the Centre for Brain and Cognitive Development, Birkbeck College, University of London. We are grateful to all the families who participated in this research and all the undergraduate students who assisted with data collection.

Declaration of Interests

The authors declare that the research was conducted in the absence of any commercial or financial relationships that could be construed as a potential conflict of interest.

Data availability statement

The data contains human subject data from minors and guardians provided informed consent to having data shared only with researchers involved in the project, in anonymised form. A Patient and Public Involvement (PPI) initiative at the Centre for Brain and Cognitive Development aimed to actively work in partnership with parents and guardians participating in research studies to help design and manage future research. A comprehensive public survey was conducted as part of this initiative which aimed to evaluate parent attitudes to data sharing in developmental science. This survey revealed that majority of parents do not want their data to be shared openly but are open to the data being shared with other researchers related to the project. Therefore, in order to adhere to participant preference/choice, a curated data sharing approach must be followed wherein the data can only be made available upon reasonable request through a formal data sharing and project affiliation agreement. The researcher will have to contact MFS and complete a project affiliation form providing their study aims, a detailed study proposal, plan for the analysis protocol, ethics, and plans for data storage and protection. Successful proposals will have aims aligned with the aims of the original study. Raw NIRS data, EEG data and integrated NIRS-EEG data can be made available in anonymised form. ID numbers linking the NIRS and EEG data, however, cannot be provided as parents/guardians have consented only to data being shared in anonymised form. All code used to analyse the NIRS data and the integration of the NIRS and EEG data is available on GitHub (https://github.com/maheensiddiqui91/NIRS-EEG). EEG data was processed using EEGlab which is a publicly available toolbox.

Methods

Participants: The study protocol was approved by the Birkbeck Ethics Committee, ethics approval number 161747. Participants were forty-two 4-to-7-month-old infants (mean age: 179± 16 days; 22 males and 20 females); parents provided written informed consent to participate in the study, for the publication of the research and additionally for the publication and use of any photographs taken during the study of the infant wearing the NIRS-EEG headgear. Inclusion criteria included term birth (37 – 40 weeks); exclusion criteria included known presence or family history of developmental disorders. The sample size was determined by performing a power analysis of existing data using G*Power.

Experimental Procedure: The experimental stimuli were designed using Psychtoolbox in Matlab (Mathworks, USA) and consisted of social and non-social videos. The social videos consisted of a variety of full-colour video clips of actors performing nursery rhymes such as "pat-a-cake" and "wheels on the bus". The non-social videos consisted of dynamic video clips of moving mechanical toys. The visual and auditory components of both social and non-social videos was matched. These videos have been used extensively in prior infant studies in both EEG studies [3] and NIRS studies [89], [90]. Both social and non-social experimental conditions were presented alternatingly for a varying duration between 8-12 s. The baseline condition consisted of static transport images, for example cars and helicopters, which were presented for a pseudorandom duration of 1 – 3 s each for a total of 8 s. Following the presentation of the baseline condition, a fixation cross in the shape of a ball or a flower appeared in the centre of the screen to draw the infant's attention back to the screen in case the infant had become bored during the baseline period. The following experimental condition was then presented once the infant's attention was on the fixation cross. **Error! Reference source not found.**a depicts the order of stimulus presentation. All infants sat in their parent's lap at an approximate distance of 65 cm from a 35-in screen which was used to display the experimental stimuli. The study began with a minimum 10 s rest period to draw the infant's attention towards the screen during which the infant was presented with various shapes in the four corners of the screen. Following this, the baseline and experimental stimuli were presented alternatingly until the infant became bored or fussy.

Data acquisition and array placement: bNIRS and EEG data was acquired simultaneously and the bNIRS optodes and EEG electrodes were positioned on the head using custom-built, 3-D printed arrays which were embedded within a soft neoprene cap (Neuroelectrics, Spain). Figures 5a and 5b show the locations of bNIRS optodes and EEG electrodes on the head. Figure 1b shows the combined bNIRS-EEG headgear positioned on an infant. The array was designed to allow measurement from several cortical regions which included occipital, parietal, temporal, and central regions to allow investigation of neurovascular coupling in different cortical regions that are expected to be activated by dynamic stimuli.

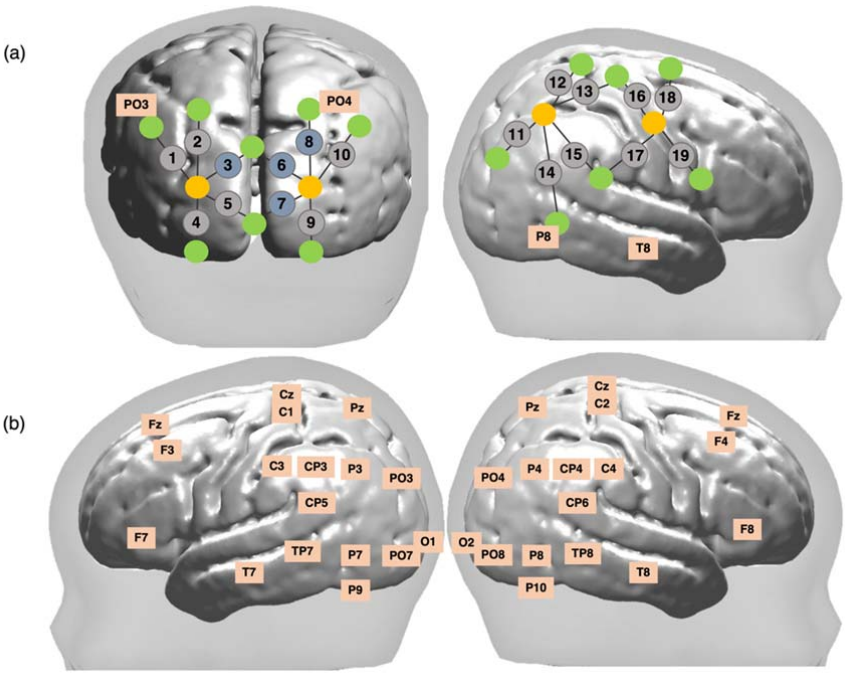

Figure 5: Schematic representation of bNIRS and EEG channel locations. (a) Locations of bNIRS channels (grey circles) over the occipital cortex and the right hemisphere and locations of the bNIRS sources (orange circles) and detectors (green circles) relative to EEG 10/20 locations. Channels shown in blue (3, 6, 8 and 10) were excluded from the analysis (b) Locations of the 32 EEG electrodes.

Broadband NIRS: Brain haemodynamic ($\Delta[HbO_2]$, $\Delta[HHb]$) and metabolic changes ($\Delta[oxCCO]$) were measured using an in-house broadband NIRS system developed at University College London [91]. The bNIRS system consisted of two light sources that consisting of halogen light bulbs (Phillips) that emitted light in the near-infrared range (504 – 1068 nm). The light was directed to the infant's head through customised bifurcated optical fibres (Loptek, Germany), allowing each light source to split into two pairs of light sources. This formed a total of four light sources at the participant-end and each pair of light sources were controlled by a time multiplexing mechanism whereby one pair of light sources was on every 1.4 s. The system also consisted of fourteen detector fibres at the participant-end which were connected to two spectrometers, seven for each spectrometer (in-house developed lens spectrographs and PIXIS512f CCD cameras (Princeton Instruments). The configuration of four light sources and fourteen detectors formed a total of nineteen measurement channels. These were positioned over the occipital cortex and the right hemisphere as shown in Figure 5a. The source-detector separation was 2.5 cm.

Data were analysed in Matlab (Mathworks, USA) using in-house scripts. First, for each participant, across all wavelengths, wavelet-based motion correction [92] was applied to the attenuation change signal to correct for motion artifacts. The tuning parameter $\alpha = 0.8$ was used. Following this, the UCLn algorithm [4] was used with a wavelength-dependent, age-appropriate fixed differential path-length factor (DPF) value of 5.13 [93]. While the light sources emitted light between 504 – 1068 nm, the changes in concentration of HbO_2, HHb and oxCCO were calculated using 120 wavelengths between 780 – 900 nm. A 4^{th}-order bandpass Butterworth filter from 0.01 – 0.4 Hz was used to filter the data. For each infant, channels were assessed for signal quality and any channels with poor signal quality were

rejected. Following this, the HbO_2, HHb and oxCCO time-series were entered into a General Linear Model (GLM) to correlate bNIRS and EEG data.

For each infant, intensity counts (or photon counts) from each of the fourteen detectors were used to assess the signal-to-noise (SNR) ratio at each channel and the channels with intensity counts lower than 2000 or higher than 40,000 were excluded [91]. If an infant had more than 60% of channels excluded, they were excluded from the study. At the group level, five channels over the occipital cortex were excluded due to poor SNR in majority of infants (Channel 3 excluded in 64% of infants, Channel 6 excluded in 83% of infants, Channel 7 excluded in 64% of infants, Channel 8 excluded in 79% of infants) and one channel over the right hemisphere was excluded in 100% of infants due to a damaged optical fibre. The average number of blocks included at each channel was 6.

EEG: EEG was used to measure neural activity simultaneously to haemodynamic and metabolic activity using the Enobio EEG system (Neuroelectrics, Spain) which is a wireless gel-based system. The system consisted of 32 electrodes, the locations of which are shown in Figure 5b. The sampling rate of the system was 500 Hz. The experimental protocol in Psychtoolbox sent event markers to both bNIRS and EEG systems using serial port communication which was then used to synchronise the bNIRS and EEG.

All data were analysed using the EEGlab Toolbox (Schwartz Centre for Computation Neuroscience, UC San Diego, USA) and in-house scripts in Matlab (Mathworks, USA). The raw EEG signal was band-pass filtered between 0.1 – 100 Hz and a notch filter (48 – 52 Hz) was applied to remove artifacts due to line noise. Following this, blocks of the data were created such that they consisted of the baseline period prior to the stimulus presentation and the entire following stimulus period. These blocks were then segmented into 1 s segments such that for both the baseline and the stimulus, each 8 – 12 s presentation of the baseline condition or the stimulus condition yielded 8 – 12 x 1 s segments. These 1 s segments consisted of 200 ms of the previous 1 s segment and 800 ms of the current segment and the 200 ms was used for baseline correction of each 1 s segment. This will be referred to as "within-segment baseline correction" from here. Segments where the infants were not visually attending to the stimulus were removed. An average of 30 x 1 s segments were included per infant. Artifacts were detected using automatic artifact-detection in EEGlab and through manual identification. EEG segments were rejected if the signal amplitude exceeded 200 μV, or if electro-ocular, movement, or muscular artifacts occurred. Channels with noisy data were interpolated by an algorithm incorporated within EEGlab. Data were then re-referenced to the average reference.

Within each block (consisting of the baseline period and the stimulus period), each artifact-free 1 s segment was subjected to a power analysis to calculate the average root mean square (RMS) power for both low and high frequency bands – theta (3 – 6 Hz), alpha (8 – 12 Hz), beta (13 – 30 Hz), gamma (20 – 60 Hz) and high gamma (60 – 80 Hz), within each 1 s segment. This then yielded the average RMS power across the block (baseline period + following stimulus period). Baseline correction was performed by subtracting the average of the 2 s of the baseline period from the entire block. This will be referred to as the "block baseline correction" from here on. RMS power was chosen as the metric to correlate bNIRS and EEG data as previous studies have demonstrated that task-related BOLD changes are best explained by RMS [94], [95]. The blocks were then averaged across trials to obtain an averaged RMS response per participant. A portion of the averaged RMS power was then entered into a GLM analysis described below – this consisted of 8 seconds of the stimulus

period. Figure 6 supplement 1 provides a visual depiction of how the RMS power was derived from the pre-processed EEG data. For each participant, the RMS power was also averaged across the stimulus period for statistical analysis of the EEG data. For each frequency band, statistical t-tests were performed on this averaged RMS power comparing the social condition versus the baseline (RMS power was averaged during the baseline period), the non-social condition versus the baseline and social versus non-social. The false discovery rate (FDR) procedure using the Benjamin Hochberg method [96] as performed to correct for multiple comparisons, across the 32 EEG channels.

Data Analysis: Figure 6 supplement 2 outlines the data analysis pipelines for both bNIRS and EEG data, as well as the procedure for the combined bNIRS-EEG analysis.

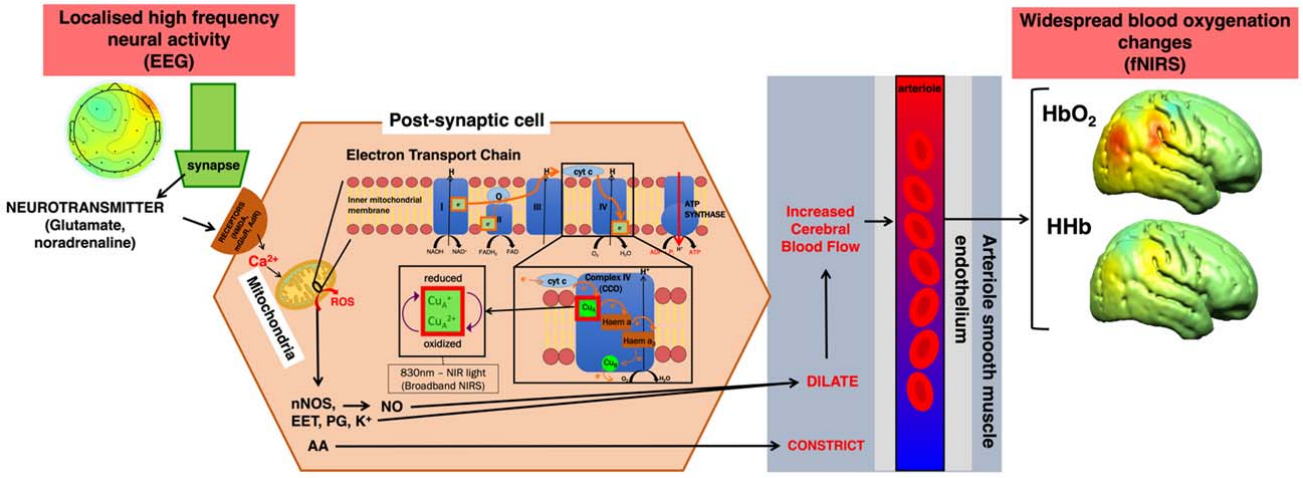

Figure 6: Simplified summary of the signalling pathways that mediate neurovascular coupling. High-frequency neural activity causes the release *of neurotransmitters such as* glutamate *and noradrenaline* which *bind* to *either* N-methyl-D-aspartate (NMDA) receptors in interneurons *or metabotropic glutamate receptors (mGluR) or adrenaline receptors in astrocytes. In both cases, this* causes an influx of calcium (Ca^{2+}) which in turn leads to an increase in ATP production through the mitochondrial electron transport chain (ETC). As a by-product, *in interneurons,* nitric oxide (NO) *is* produced *in the interneurons which* dilates arterioles to increase blood flow leading to increased oxygen delivery in surrounding brain regions. *Alternatively, in astrocytes derivates of arachidonic acid (AA) which include prostaglandins (PG) and epoxyeicosatrienoic acids (EET) which cause vasodilation*

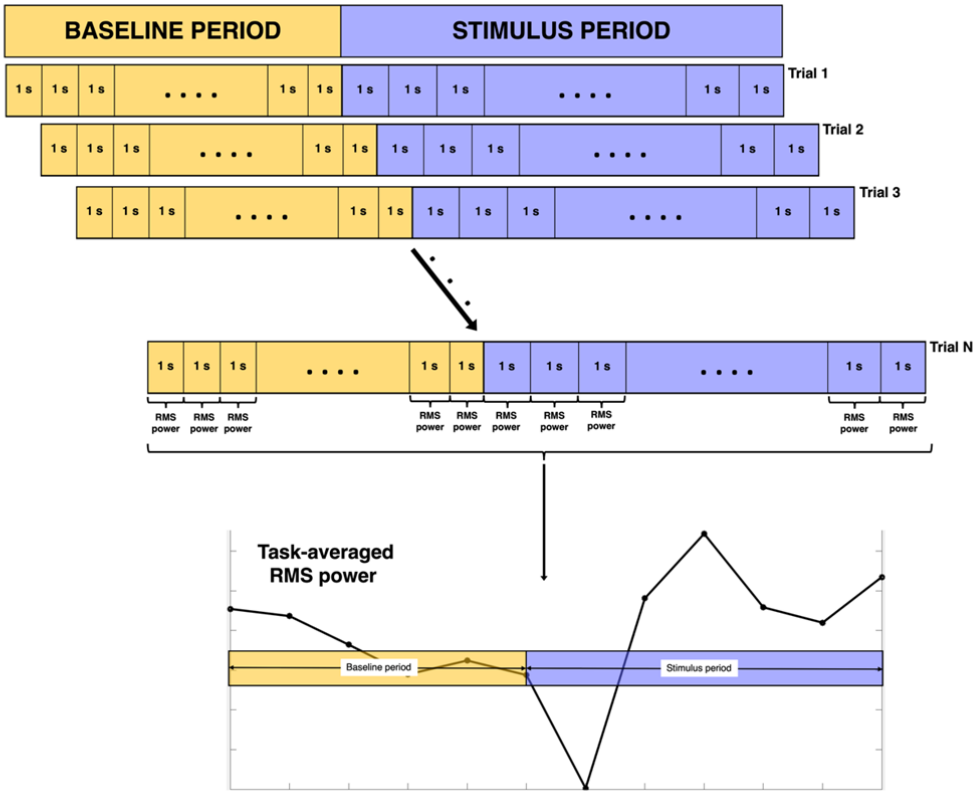

Figure 6 supplement 1: Procedure for deriving the EEG RMS power from the pre-processed EEG data. Each 1 s segment is made up of 200 ms of the previous segment and 800 ms of the current segment. The task-averaged RMS power shown here is average theta power across all infants from a single channel for the purposes of outlining the procedure.

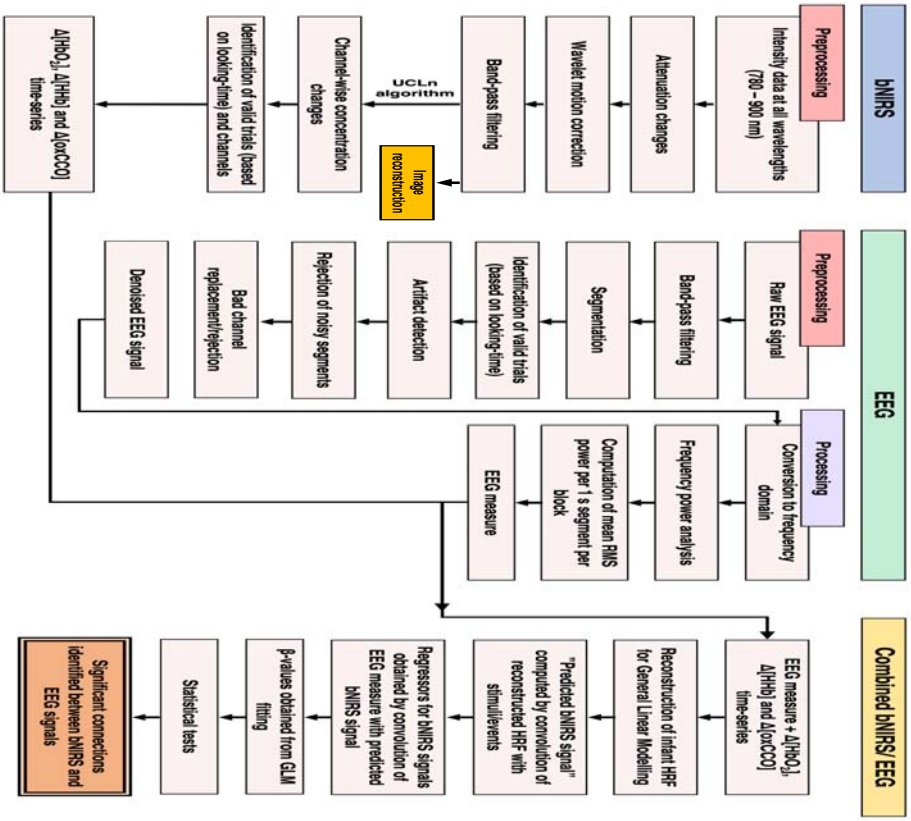

Figure 6 supplement 2: Flow chart for the data analysis pipelines for bNIRS (left), EEG (middle) and combined bNIRS-EEG (right).

Combined NIRS-EEG analysis: A GLM [97] approach was employed to investigate the relationship between the bNIRS hemodynamic and metabolic data with the EEG neural data. The canonical GLM typically uses a model of the expected haemodynamic response, i.e. the hemodynamic response function (HRF), to predict the hemodynamic signal. However, given the differences in the haemodynamic response in adults and infants, the standard adult HRF model cannot be assumed for infant data. For example, infants display a delay in their haemodynamic responses [98]–[100]. In addition, the analogous of the HRF is not established for the metabolic response (i.e. the metabolic response function or MRF). Therefore, the first step of this analysis involved reconstructing the HRF for HbO_2 and HHb and the MRF for oxCCO before combing bNIRS and EEG data.

The reconstruction of the infant HRF and MRF started with block-averaging the HbO_2, HHb, and oxCCO signals for social and non-social conditions within each infant. Based on our previous study [19], we selected only the channels that displayed statistically significant responses to the contrast task versus baseline. The single subjects block-averaged responses were averaged across the social and non-social conditions and then across the significant channels. The resulting block-averaged responses were then averaged across the group to obtain a "grand average" HbO_2, HHb and oxCCO response.

The grand average was then used in an iterative approach to estimate the HRF and MRF that best fit the HbO_2, HHb and oxCCO responses. This involved fitting the grand averaged signals with different HRF/MRF models starting from the canonical HRF made of two gamma functions and varying the following parameters: 1) delay of response, 2) delay of the

undershoot and 3) ratio of response to undershoot to identify the combination of parameters that best reconstructed the infant HRF/MRF for the social/non-social stimuli. The parameters were varied in increments of 1 s such that the delay of the response was varied from 5 s to 15 s from the stimulus onset, the delay of the undershoot was varied from 5 to 20 s and the ratio of the response to the undershoot was varied from 2 to 6 s. All possible combinations of parameters were tested. The grand average responses were fitted with each HRF/MRF in GLM approach, and β-values were obtained for each combination of the HRF/MRF parameters. The β-values were entered into a statistical test and the parameter combinations that yielded the highest, statistically significant β-values (i.e. the model best fitting the data) were selected to reconstruct the infant HRF/MRF. This is approach is similar to those used previously to reconstruct the infant HRF [100] and identified the best fit to be with a 2-s delay of response for HbO_2 and HHb and a 3-s delay of response for oxCCO in comparison to the adult HRF (i.e. 6 s). Moreover, the delay of the undershoot was 9-s earlier for all chromophores and the ratio of the response to the undershoot was 2 for HbO_2 and HHb and 3 for oxCCO, in comparison to 6 for the adult HRF. These correspond to the basis function representing the hemodynamic/metabolic response to an event of zero duration/impulse function. The new reconstructed HRF and MRF were then used for the GLM approach to correlate bNIRS and EEG data. The process for estimating the HRF and MRF has been depicted in Figure 7.

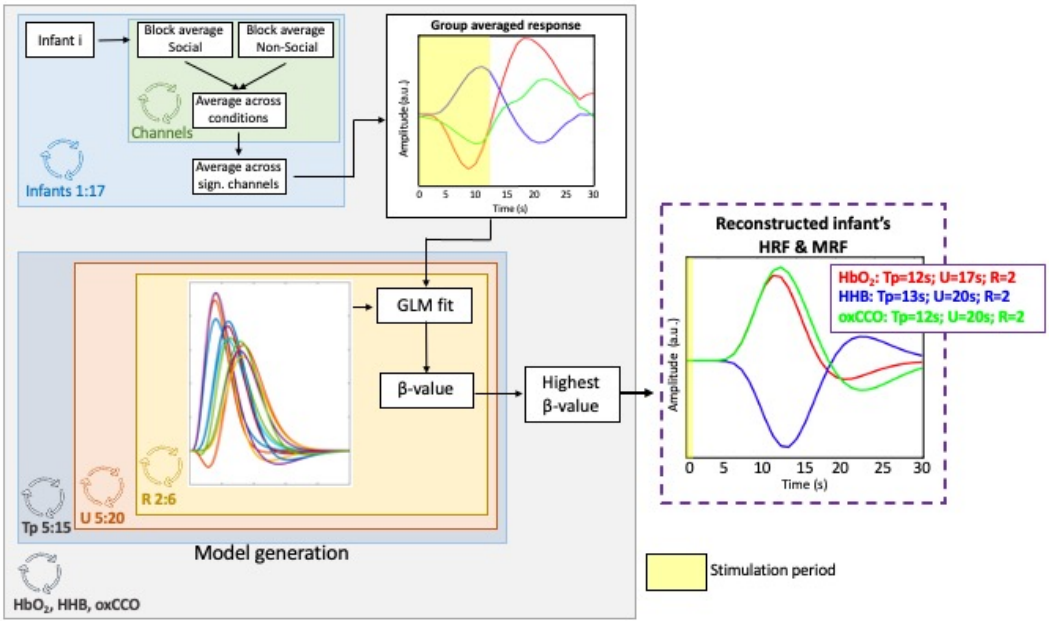

Figure 7: Procedure for obtaining the reconstructed haemodynamic response function (HRF) and the metabolic response function (MRF). The panel on the right shows the estimated HRF and MRF with the corresponding basis function parameters giving the best fit with the group averaged HbO_2, HHb, oxCCO responses. The yellow shaded areas represent the stimulation periods.

To constrain the analysis, we chose to investigate coupling of haemodynamic and metabolic with neural activity at specific channels. For this, we used the results from an analysis we described previously that combined bNIRS haemodynamic and metabolic signals [19], [101]. The results from this identified task-relevant cortical regions that displayed high levels of haemodynamic and metabolic coupling. The bNIRS channels that displayed significant haemodynamic and metabolic coupling for social and non-social conditions were used here. All EEG channels were used as EEG is not as spatially specific as bNIRS. For each infant, for each chromophore, for each channel and each EEG frequency band, the new infant

HRF/MRF that was reconstructed in the previous step was convolved with the events to obtain the "predicted" bNIRS signal. The "predicted" bNIRS signal was then convolved with the EEG RMS power block (consisting only of the data from the stimulus period) at each frequency band to obtain the neural regressor for the bNIRS data, considering both social and non-social conditions together. The design matrix thus included the neural regressor reflecting the increased in EEG activity to the social and non-social stimuli and used to fit the bNIRS data. This was performed for HbO2, HHb, and oxCCO individually for all the channels. β-values were estimated for each channel and t-tests against 0 were conducted to test whether there was a statistically significant association between bNIRS signals and EEG frequency bands. The false discovery rate (FDR) procedure using the Benjamin Hochberg method [96] was performed to correct for multiple comparisons across EEG and bNIRS channels. The FDR-corrected significant t-values were plotted. This method has been used in numerous studies previously in correlating fMRI BOLD – EEG [21]. Only bNIRS channels that displayed significant (prior to FDR correction) haemodynamic and metabolic coupling were used for this analysis (as indicated in Figure and **Error! Reference source not found.**). For the social condition, channels 12, 13 and 14 for HbO_2, channels 11, 12, 14 and 18 for HHb and channels 11, 12, 13, 14 and 18 for oxCCO displayed significant haemodynamic and metabolic coupling. Moreover, for the non-social condition, channels 12 and 14 for HbO_2, channels 12, 14 and 16 for HHb and channels 12, 14 and 16 for oxCCO displayed significant coupling. For consistency, the channels selected for the bNIRS-EEG analysis were the same across chromophores and conditions. The final channels included in the analysis therefore were channels 11, 12, 13, 14, 16 and 18. For the integrated bNIRS-EEG analysis, 6 channel-wise t-tests were carried (one per included bNIRS channel, e.g. 6) for each EEG frequency band. Therefore, the FDR correction was applied across the 6 bNIRS channels for each of the hypotheses tested.

For the bNIRS analysis, data from 25 infants was included while for the EEG analysis, data from 35 infants were included. For the joint bNIRS-EEG analysis, only infants that had both valid bNIRS and EEG data for both social and non-social conditions were included and therefore 14 infants were included in this analysis.

Image reconstruction: Image reconstruction was performed on the bNIRS data, at the individual subject level and then averaged across infants to produce a grand average that is shown in Figure 4. This was done to visually assess the similarities in the spatial distributions of the changes in HbO_2, HHb, oxCCO. For this analysis, three additional long-distance channels were created over the right hemisphere (in addition to the 19 bNIRS channels) that had a source/detector separation of 4.3cm to generate multiple and overlapping channels.

More precisely, the block averaged attenuation changes at 13 discrete wavelengths (from 780 – 900 nm at 10 nm intervals) for each infant were selected from the bNIRS data. This was done to reduce the computational burden of the reconstruction [102]. A four-layer infant head-model (consisting of the grey matter (GM), white matter (WM), cerebrospinal fluid (CSF) and extra cerebral tissue) was built using averaged MRI data from a cohort of 12-month-old infants presented in Shi et al. [103]. The Betsurf segmentation procedure [104] was then used to define an outer scalp boundary from the average head MRI template. The voxelised four-layer model was converted to a high-resolution tetrahedral mesh ($\sim 7.8 \times 10^5$ nodes and $\sim 4.7 \times 10^6$ elements) using the iso2mesh software (Fang & Boas, 2009). The same software was used to create the GM surface mesh ($\sim 5.8 \times 10^4$ nodes and $\sim 1.2 \times 10^5$ faces), used to visualise the reconstructed images.

The reconstruction of images of HbO_2, HHb and ΔoxCCO are described elsewhere [105], using a multispectral approach [106]. Wavelength-specific Jacobians were computed with the Toast++ software [107] on the tetrahedral head mesh and projected onto a 50 × 60 × 50 voxel regular grid for reconstruction, using an intermediate finer grid of 100 × 120 × 100 voxels to optimize the mapping between mesh and voxel space. Optical properties were assigned to each tissue type and for each wavelength by fitting all published values for these tissue types [108]–[110]. Diffuse boundary sources and detectors were simulated as a Gaussian profile with a 2-mm standard deviation, and Neumann boundary conditions were applied. The inverse problem was solved employing the LSQR method to solve the matrix equations resulting from the minimization and using first-order Tikhonov regularization, with the parameter covariance matrix containing the diagonal square matrices with the background concentration values of the three chromophores (23.7 for HbO_2, 16 for HHb and 6 for ΔoxCCO) [111], [112] and the noise covariance matrix set as the identity matrix. The maximum number of iterations allowed to the LSQR method was set to 50, and with a tolerance of 10^{-5}. The regularization hyperparameter λ was set to 10^{-2}.

The reconstructed images, defined on the same regular grid of the Jacobian, were remapped to the tetrahedral head mesh and then projected to the GM surface mesh, by assigning a value to each node on the GM boundary surface that was equal to the mean value of all the tetrahedral mesh node values within a 3-mm radius. The concentration changes for HbO_2 and HHb were normalised to the maximum concentration change of HbO_2 while ΔoxCCO was normalised to its own maximum change in concentration.

References

[1] M. H. Johnson, "Functional brain development in humans," *Nat. Rev. Neurosci.*, vol. 2, no. 7, pp. 475–483, Jul. 2001, doi: 10.1038/35081509.

[2] M. H. Johnson, "Interactive Specialization: A domain-general framework for human functional brain development?," *Developmental Cognitive Neuroscience*, vol. 1, no. 1. pp. 7–21, 2011, doi: 10.1016/j.dcn.2010.07.003.

[3] E. J. H. Jones, K. Venema, R. Lowy, R. K. Earl, and S. J. Webb, "Developmental changes in infant brain activity during naturalistic social experiences," *Dev. Psychobiol.*, vol. 57, no. 7, pp. 842–853, Nov. 2015, doi: 10.1002/dev.21336.

[4] G. Bale, C. E. Elwell, and I. Tachtsidis, "From Jöbsis to the present day: a review of clinical near-infrared spectroscopy measurements of cerebral cytochrome-c-oxidase," *J. Biomed. Opt.*, vol. 21, no. 9, p. 91307, 2016, [Online]. Available: http://dx.doi.org/10.1117/1.JBO.21.9.091307.

[5] D. Attwell and C. Iadecola, "The neural basis of functional brain imaging signals," *Trends Neurosci.*, vol. 25, no. 12, pp. 621–625, 2002, doi: 10.1016/S0166-2236(02)02264-6.

[6] G. Buzsáki, *Rhythms of the Brain*. Oxford University Press, 2006.

[7] M. E. Raichle and M. A. Mintun, "Brain work and brain imaging.," *Annu. Rev. Neurosci.*, vol. 29, pp. 449–476, 2006, doi: 10.1146/annurev.neuro.29.051605.112819.

[8] L. Sokoloff, "Energetics of functional activation in neural tissues.," *Neurochem. Res.*, vol. 24, no. 2, pp. 321–329, Feb. 1999, doi: 10.1023/a:1022534709672.

[9] P. Steiner, "Brain Fuel Utilization in the Developing Brain.," *Ann. Nutr. Metab.*, vol. 75 Suppl 1, pp. 8–18, 2019, doi: 10.1159/000508054.

[10] R. Leech, G. Scott, R. Carhart-Harris, F. Turkheimer, S. D. Taylor-Robinson, and D. J. Sharp, "Spatial Dependencies between Large-Scale Brain Networks," *PLoS One*, vol. 9, no. 6, pp. 1–10, 2014, doi: 10.1371/journal.pone.0098500.

[11] S. Vaynman, Z. Ying, A. Wu, and F. Gomez-Pinilla, “Coupling energy metabolism with a mechanism to support brain-derived neurotrophic factor-mediated synaptic plasticity.,” *Neuroscience*, vol. 139, no. 4, pp. 1221–1234, 2006, doi: 10.1016/j.neuroscience.2006.01.062.

[12] M. Kozberg and E. Hillman, “Neurovascular coupling and energy metabolism in the developing brain,” in *Progress in Brain Research*, vol. 225, 2016, pp. 213–242.

[13] H. L. Kosakowski, M. A. Cohen, A. Takahashi, B. Keil, N. Kanwisher, and R. Saxe, “Selective responses to faces, scenes, and bodies in the ventral visual pathway of infants.,” *Curr. Biol.*, vol. 32, no. 2, pp. 265-274.e5, Jan. 2022, doi: 10.1016/j.cub.2021.10.064.

[14] T. Farroni *et al.*, “Infant cortex responds to other humans from shortly after birth,” *Sci. Rep.*, 2013, doi: 10.1038/srep02851.

[15] T. Grossmann, R. Oberecker, S. P. Koch, and A. D. Friederici, “The Developmental Origins of Voice Processing in the Human Brain,” *Neuron*, vol. 65, no. 6, pp. 852–858, 2010, doi: https://doi.org/10.1016/j.neuron.2010.03.001.

[16] S. Lloyd-Fox, A. Blasi, E. Mercure, C. E. Elwell, and M. H. Johnson, “The emergence of cerebral specialization for the human voice over the first months of life,” *Soc. Neurosci.*, vol. 7, no. 3, pp. 317–330, May 2012, doi: 10.1080/17470919.2011.614696.

[17] S. Lloyd-Fox, A. Blasi, C. E. Elwell, T. Charman, D. Murphy, and M. H. Johnson, “Reduced neural sensitivity to social stimuli in infants at risk for autism,” *Proc. R. Soc. B Biol. Sci.*, vol. 280, no. 1758, p. 20123026, May 2013, doi: 10.1098/rspb.2012.3026.

[18] S. Lloyd-Fox *et al.*, “Cortical responses before 6 months of life associate with later autism,” *Eur. J. Neurosci.*, Nov. 2017, doi: 10.1111/ejn.13757.

[19] M. F. Siddiqui *et al.*, “Regional Haemodynamic and Metabolic Coupling in Infants,” *Front. Hum. Neurosci.*, vol. 15, 2022, doi: 10.3389/fnhum.2021.780076.

[20] R. Scheeringa *et al.*, “Neuronal Dynamics Underlying High- and Low-Frequency EEG Oscillations Contribute Independently to the Human BOLD Signal,” *Neuron*, vol. 69, no. 3, pp. 572–583, Feb. 2011, doi: 10.1016/j.neuron.2010.11.044.

[21] R. Scheeringa, K. M. Petersson, R. Oostenveld, D. G. Norris, P. Hagoort, and M. C. M. Bastiaansen, “Trial-by-trial coupling between EEG and BOLD identifies networks related to alpha and theta EEG power increases during working memory maintenance,” *Neuroimage*, vol. 44, no. 3, pp. 1224–1238, Feb. 2009, doi: 10.1016/j.neuroimage.2008.08.041.

[22] R. I. Goldman, J. M. Stern, J. Engel, and M. S. Cohen, “Simultaneous EEG and fMRI of the alpha rhythm,” *Neuroreport*, 2002, doi: 10.1097/00001756-200212200-00022.

[23] H. Yuan, T. Liu, R. Szarkowski, C. Rios, J. Ashe, and B. He, “Negative covariation between task-related responses in alpha/beta-band activity and BOLD in human sensorimotor cortex: An EEG and fMRI study of motor imagery and movements,” *Neuroimage*, vol. 49, no. 3, pp. 2596–2606, Feb. 2010, doi: 10.1016/J.NEUROIMAGE.2009.10.028.

[24] J. Niessing, “Hemodynamic Signals Correlate Tightly with Synchronized Gamma Oscillations,” *Science (80-.).*, vol. 309, no. 5736, pp. 948–951, Aug. 2005, doi: 10.1126/science.1110948.

[25] N. K. Logothetis, J. Pauls, M. Augath, T. Trinath, and A. Oeltermann, “Neurophysiological investigation of the basis of the fMRI signal,” *Nature*, vol. 412, no. 6843, pp. 150–157, Jul. 2001, doi: 10.1038/35084005.

[26] S. P. Koch, P. Werner, J. Steinbrink, P. Fries, and H. Obrig, “Stimulus-Induced and State-Dependent Sustained Gamma Activity Is Tightly Coupled to the Hemodynamic Response in Humans,” *J. Neurosci.*, vol. 29, no. 44, pp. 13962 LP – 13970, Nov. 2009, doi: 10.1523/JNEUROSCI.1402-09.2009.

[27] T. Wilcox, J. A. Haslup, and D. A. Boas, “Dissociation of processing of featural and spatiotemporal information in the infant cortex,” *Neuroimage*, 2010, doi: 10.1016/j.neuroimage.2010.06.064.
[28] T. Dekker, D. Mareschal, M. I. Sereno, and M. H. Johnson, “Dorsal and ventral stream activation and object recognition performance in school-age children,” *Neuroimage*, 2011, doi: 10.1016/j.neuroimage.2010.11.005.
[29] P. Pinti, M. F. Siddiqui, A. D. Levy, E. J. H. Jones, and I. Tachtsidis, “An analysis framework for the integration of broadband NIRS and EEG to assess neurovascular and neurometabolic coupling,” *Sci. Rep.*, 2021, doi: 10.1038/s41598-021-83420-9.
[30] Y. Wang *et al.*, “Long-range connections mirror and link microarchitectural and cognitive hierarchies in the human brain,” *bioRxiv*, 2021, doi: 10.1101/2021.10.25.465692.
[31] R. Scheeringa, K. M. Petersson, A. Kleinschmidt, O. Jensen, and M. C. M. Bastiaansen, “EEG Alpha Power Modulation of fMRI Resting-State Connectivity,” *Brain Connect.*, 2012, doi: 10.1089/brain.2012.0088.
[32] M. T. Kucewicz *et al.*, “High frequency oscillations are associated with cognitive processing in human recognition memory,” *Brain*, vol. 137, no. 8, pp. 2231–2244, Aug. 2014, doi: 10.1093/brain/awu149.
[33] J. J. Harris, C. Reynell, and D. Attwell, “The physiology of developmental changes in BOLD functional imaging signals,” *Dev. Cogn. Neurosci.*, vol. 1, no. 3, pp. 199–216, Jul. 2011, doi: 10.1016/j.dcn.2011.04.001.
[34] R. A. Rowan and D. S. Maxwell, “Patterns of vascular sprouting in the postnatal development of the cerebral cortex of the rat,” *Am. J. Anat.*, vol. 160, no. 3, pp. 247–255, Mar. 1981, doi: 10.1002/aja.1001600303.
[35] M. G. Norman and J. R. O’Kusky, “The growth and development of microvasculature in human cerebral cortex,” *J. Neuropathol. Exp. Neurol.*, vol. 45, no. 3, pp. 222–232, May 1986, doi: 10.1097/00005072-198605000-00004.
[36] C. M. Zehendner, S. Tsohataridis, H. J. Luhmann, and J. W. Yang, “Developmental switch in neurovascular coupling in the immature rodent barrel cortex,” *PLoS One*, vol. 8, no. 11, p. e80749, Nov. 2013, doi: 10.1371/journal.pone.0080749.
[37] M. G. Kozberg, B. R. Chen, S. E. DeLeo, M. B. Bouchard, and E. M. C. Hillman, “Resolving the transition from negative to positive blood oxygen level-dependent responses in the developing brain,” *Proc. Natl. Acad. Sci.* , vol. 110, no. 11, pp. 4380–4385, Mar. 2013, doi: 10.1073/pnas.1212785110.
[38] B. R. Chen, M. G. Kozberg, M. B. Bouchard, M. A. Shaik, and E. M. C. Hillman, “A Critical Role for the Vascular Endothelium in Functional Neurovascular Coupling in the Brain,” *J. Am. Heart Assoc.*, vol. 3, no. 3, pp. e000787–e000787, Jun. 2014, doi: 10.1161/JAHA.114.000787.
[39] K. Fujimoto, “Pericyte-endothelial gap junctions in developing rat cerebral capillaries: A fine structural study,” *Anat. Rec.*, vol. 242, no. 4, pp. 562–565, Aug. 1995, doi: 10.1002/ar.1092420412.
[40] A. Seregi, M. Keller, and G. Hertting, “Are cerebral prostanoids of astroglial origin? Studies on the prostanoid forming system in developing rat brain and primary cultures of rat astrocytes,” *Brain Res.*, vol. 404, no. 1–2, pp. 113–120, 1987, doi: 10.1016/0006-8993(87)91361-8.
[41] C. C. Stichel, C. M. M□ller, and K. Zilles, “Distribution of glial fibrillary acidic protein and vimentin immunoreactivity during rat visual cortex development,” *J. Neurocytol.*, vol. 20, no. 2, pp. 97–108, Feb. 1991, doi: 10.1007/BF01279614.
[42] H. T. Chugani, M. E. Phelps, and J. C. Mazziotta, “Positron emission tomography study of human brain functional development,” *Ann. Neurol.*, vol. 22, no. 4, pp. 487–

497, Oct. 1987, doi: 10.1002/ana.410220408.
[43] M. Kozberg and E. Hillman, “Chapter 10 – Neurovascular coupling and energy metabolism in the developing brain,” in *Progress in Brain Research*, vol. 225, Elsevier, 2016, pp. 213–242.
[44] D. Malonek and A. Grinvald, “Interactions between electrical activity and cortical microcirculation revealed by imaging spectroscopy: Implications for functional brain mapping,” *Science (80-.).*, 1996, doi: 10.1126/science.272.5261.551.
[45] P. Phan, D. Highton, J. Lai, M. Smith, C. Elwell, and I. Tachtsidis, “Multi-channel multi-distance broadband near- infrared spectroscopy system to measure the spatial response of cellular oxygen metabolism and tissue oxygenation,” *Biomed. Opt. Express*, vol. 7, no. 4424, 2016, doi: 10.1364/BOE.7.004424.
[46] M. T. T. Wong-Riley *et al.*, “Cytochrome oxidase in the human visual cortex: Distribution in the developing and the adult brain,” *Vis. Neurosci.*, vol. 10, no. 01, p. 41, Jan. 1993, doi: 10.1017/S0952523800003217.
[47] R. F. Hevner, S. Liu, and M. T. T. Wong-Riley, “A metabolic map of cytochrome oxidase in the rat brain: Histochemical, densitometric and biochemical studies,” *Neuroscience*, 1995, doi: 10.1016/0306-4522(94)00514-6.
[48] S. Uono *et al.*, “Time course of gamma-band oscillation associated with face processing in the inferior occipital gyrus and fusiform gyrus: A combined fMRI and MEG study,” *Hum. Brain Mapp.*, vol. 38, no. 4, pp. 2067–2079, Apr. 2017, doi: https://doi.org/10.1002/hbm.23505.
[49] A. S. Ghuman *et al.*, “Dynamic encoding of face information in the human fusiform gyrus,” *Nat. Commun.*, vol. 5, no. 1, p. 5672, 2014, doi: 10.1038/ncomms6672.
[50] M. Bayer, M. T. Rubens, and T. Johnstone, “Simultaneous EEG-fMRI reveals attention-dependent coupling of early face processing with a distributed cortical network,” *Biol. Psychol.*, vol. 132, pp. 133–142, 2018, doi: https://doi.org/10.1016/j.biopsycho.2017.12.002.
[51] M. Müller-Bardorff *et al.*, “Early brain responses to affective faces: A simultaneous EEG-fMRI study,” *Neuroimage*, vol. 178, pp. 660–667, 2018, doi: https://doi.org/10.1016/j.neuroimage.2018.05.081.
[52] V. T. Nguyen and R. Cunnington, “The superior temporal sulcus and the N170 during face processing: Single trial analysis of concurrent EEG–fMRI,” *Neuroimage*, vol. 86, pp. 492–502, 2014, doi: https://doi.org/10.1016/j.neuroimage.2013.10.047.
[53] V. T. Nguyen, M. Breakspear, and R. Cunnington, “Fusing concurrent EEG–fMRI with dynamic causal modeling: Application to effective connectivity during face perception,” *Neuroimage*, vol. 102, pp. 60–70, 2014, doi: https://doi.org/10.1016/j.neuroimage.2013.06.083.
[54] A. D. Engell and G. McCarthy, “The Relationship of Gamma Oscillations and Face-Specific ERPs Recorded Subdurally from Occipitotemporal Cortex,” *Cereb. Cortex*, vol. 21, no. 5, pp. 1213–1221, May 2011, doi: 10.1093/cercor/bhq206.
[55] F. Bossi, I. Premoli, S. Pizzamiglio, S. Balaban, P. Ricciardelli, and D. Rivolta, “Theta- and Gamma-Band Activity Discriminates Face, Body and Object Perception,” *Front. Hum. Neurosci.*, vol. 14, p. 74, Mar. 2020, doi: 10.3389/fnhum.2020.00074.
[56] D. Anaki, E. Zion-Golumbic, and S. Bentin, “Electrophysiological neural mechanisms for detection, configural analysis and recognition of faces,” *Neuroimage*, vol. 37, no. 4, pp. 1407–1416, 2007, doi: https://doi.org/10.1016/j.neuroimage.2007.05.054.
[57] A. Ishai, L. Ungerleider, A. Martin, and J. Haxby, “The Representation of Objects in the Human Occipital and Temporal Cortex,” *J. Cogn. Neurosci.*, vol. 12 Suppl 2, pp. 35–51, Nov. 2000, doi: 10.1162/089892900564055.
[58] K. A. Pelphrey, J. P. Morris, and G. McCarthy, “Neural basis of eye gaze processing

deficits in autism," *Brain*, vol. 128, no. 5, pp. 1038–1048, May 2005, doi: 10.1093/brain/awh404.

[59] W. Sato *et al.*, "Rapid, high-frequency, and theta-coupled gamma oscillations in the inferior occipital gyrus during face processing," *Cortex*, vol. 60, pp. 52–68, 2014, doi: https://doi.org/10.1016/j.cortex.2014.02.024.

[60] E. Zion-Golumbic, T. Golan, D. Anaki, and S. Bentin, "Human face preference in gamma-frequency EEG activity," *Neuroimage*, vol. 39, no. 4, pp. 1980–1987, 2008, doi: https://doi.org/10.1016/j.neuroimage.2007.10.025.

[61] Z. Gao, A. Goldstein, Y. Harpaz, M. Hansel, E. Zion-Golumbic, and S. Bentin, "A magnetoencephalographic study of face processing: M170, gamma-band oscillations and source localization," *Hum. Brain Mapp.*, vol. 34, no. 8, pp. 1783–1795, Aug. 2013, doi: 10.1002/hbm.22028.

[62] A. von Stein and J. Sarnthein, "Different frequencies for different scales of cortical integration: from local gamma to long range alpha/theta synchronization," *Int. J. Psychophysiol.*, vol. 38, no. 3, pp. 301–313, 2000, doi: https://doi.org/10.1016/S0167-8760(00)00172-0.

[63] R. T. Canolty and R. T. Knight, "The functional role of cross-frequency coupling.," *Trends Cogn. Sci.*, vol. 14, no. 11, pp. 506–515, Nov. 2010, doi: 10.1016/j.tics.2010.09.001.

[64] B. van der Velde, T. White, and C. Kemner, "The emergence of a theta social brain network during infancy," *Neuroimage*, vol. 240, p. 118298, 2021, doi: https://doi.org/10.1016/j.neuroimage.2021.118298.

[65] A. J. Smith, H. Blumenfeld, K. L. Behar, D. L. Rothman, R. G. Shulman, and F. Hyder, "Cerebral energetics and spiking frequency: The neurophysiological basis of fMRI," *Proc. Natl. Acad. Sci.*, vol. 99, no. 16, pp. 10765–10770, Aug. 2002, doi: 10.1073/pnas.132272199.

[66] O. Kann, "The Energy Demand of Fast Neuronal Network Oscillations: Insights from Brain Slice Preparations ," *Frontiers in Pharmacology* , vol. 2. 2012, [Online]. Available: https://www.frontiersin.org/articles/10.3389/fphar.2011.00090.

[67] J. Niessing, B. Ebisch, K. E. Schmidt, M. Niessing, W. Singer, and R. A. W. Galuske, "Hemodynamic Signals Correlate Tightly with Synchronized Gamma Oscillations," *Science (80-.).*, vol. 309, no. 5736, pp. 948–951, Aug. 2005, doi: 10.1126/science.1110948.

[68] J. B. M. Goense and N. K. Logothetis, "Neurophysiology of the BOLD fMRI Signal in Awake Monkeys," *Curr. Biol.*, 2008, doi: 10.1016/j.cub.2008.03.054.

[69] P. S. Hosford and A. V Gourine, "What is the key mediator of the neurovascular coupling response?," *Neurosci. Biobehav. Rev.*, vol. 96, pp. 174–181, Jan. 2019, doi: 10.1016/j.neubiorev.2018.11.011.

[70] P. S. Hosford *et al.*, "CO(2) signaling mediates neurovascular coupling in the cerebral cortex.," *Nat. Commun.*, vol. 13, no. 1, p. 2125, Apr. 2022, doi: 10.1038/s41467-022-29622-9.

[71] M. C. W. Oswald *et al.*, "Reactive oxygen species regulate activity-dependent neuronal plasticity in \textit{Drosophila}," *Elife*, vol. 7, p. e39393, Dec. 2018, doi: 10.7554/eLife.39393.

[72] S. Lloyd-Fox *et al.*, "Cortical specialisation to social stimuli from the first days to the second year of life: A rural Gambian cohort," *Dev. Cogn. Neurosci.*, vol. 25, pp. 92–104, Jun. 2017, doi: 10.1016/j.dcn.2016.11.005.

[73] M. Schurz, J. Radua, M. Aichhorn, F. Richlan, and J. Perner, "Fractionating theory of mind: a meta-analysis of functional brain imaging studies.," *Neurosci. Biobehav. Rev.*, vol. 42, pp. 9–34, May 2014, doi: 10.1016/j.neubiorev.2014.01.009.

[74] M. Schurz, M. G. Tholen, J. Perner, R. B. Mars, and J. Sallet, “Specifying the brain anatomy underlying temporo-parietal junction activations for theory of mind: A review using probabilistic atlases from different imaging modalities.,” *Hum. Brain Mapp.*, vol. 38, no. 9, pp. 4788–4805, Sep. 2017, doi: 10.1002/hbm.23675.

[75] M. Corbetta and G. L. Shulman, “Control of goal-directed and stimulus-driven attention in the brain,” *Nat. Rev. Neurosci.*, vol. 3, no. 3, pp. 201–215, 2002, doi: 10.1038/nrn755.

[76] R. M. Carter and S. A. Huettel, “A nexus model of the temporal-parietal junction.,” *Trends Cogn. Sci.*, vol. 17, no. 7, pp. 328–336, Jul. 2013, doi: 10.1016/j.tics.2013.05.007.

[77] A. I. Wilterson, S. A. Nastase, B. J. Bio, A. Guterstam, and M. S. A. Graziano, “Attention, awareness, and the right temporoparietal junction,” *Proc. Natl. Acad. Sci.*, vol. 118, no. 25, p. e2026099118, 2021, doi: 10.1073/pnas.2026099118.

[78] F. Masina, R. Pezzetta, S. Lago, D. Mantini, C. Scarpazza, and G. Arcara, “Disconnection from prediction: A systematic review on the role of right temporoparietal junction in aberrant predictive processing.,” *Neurosci. Biobehav. Rev.*, vol. 138, p. 104713, Jul. 2022, doi: 10.1016/j.neubiorev.2022.104713.

[79] A. Ali, N. Ahmad, E. de Groot, M. A. J. van Gerven, and T. C. Kietzmann, “Predictive coding is a consequence of energy efficiency in recurrent neural networks,” *bioRxiv*, 2021, doi: 10.1101/2021.02.16.430904.

[80] A. HajiHosseini, A. Rodríguez-Fornells, and J. Marco-Pallarés, “The role of beta-gamma oscillations in unexpected rewards processing.,” *Neuroimage*, vol. 60, no. 3, pp. 1678–1685, Apr. 2012, doi: 10.1016/j.neuroimage.2012.01.125.

[81] M. F. Siddiqui, C. E. Elwell, and M. H. Johnson, “Mitochondrial Dysfunction in Autism Spectrum Disorders,” *Autism Open-Access*.

[82] G. Bale *et al.*, “Oxygen dependency of mitochondrial metabolism indicates outcome of newborn brain injury,” *Journal of Cerebral Blood Flow and Metabolism*, SAGE PublicationsSage UK: London, England, p. 0271678X1877792, May 18, 2018.

[83] A. Vezyroglou *et al.*, “Broadband-NIRS System Identifies Epileptic Focus in a Child with Focal Cortical Dysplasia—A Case Study,” *Metabolites* , vol. 12, no. 3. 2022, doi: 10.3390/metabo12030260.

[84] M. Jeong *et al.*, “Functional brain mapping of actual car-driving using [18F]FDG-PET,” *Ann. Nucl. Med.*, vol. 20, no. 9, pp. 623–628, 2006, doi: 10.1007/BF02984660.

[85] I. Lundgaard *et al.*, “Direct neuronal glucose uptake heralds activity-dependent increases in cerebral metabolism,” *Nat. Commun.*, vol. 6, no. 1, p. 6807, 2015, doi: 10.1038/ncomms7807.

[86] A. B. Rocher, F. Chapon, X. Blaizot, J.-C. Baron, and C. Chavoix, “Resting-state brain glucose utilization as measured by PET is directly related to regional synaptophysin levels: a study in baboons,” *Neuroimage*, vol. 20, no. 3, pp. 1894–1898, 2003, doi: https://doi.org/10.1016/j.neuroimage.2003.07.002.

[87] E. Shokri-Kojori, D. Tomasi, B. Alipanahi, C. E. Wiers, G. J. Wang, and N. D. Volkow, “Correspondence between cerebral glucose metabolism and BOLD reveals relative power and cost in human brain,” *Nat. Commun.*, 2019, doi: 10.1038/s41467-019-08546-x.

[88] S. N. Vaishnavi, A. G. Vlassenko, M. M. Rundle, A. Z. Snyder, M. A. Mintun, and M. E. Raichle, “Regional aerobic glycolysis in the human brain,” *Proc. Natl. Acad. Sci. U. S. A.*, 2010, doi: 10.1073/pnas.1010459107.

[89] S. Lloyd-Fox, A. Blasi, A. Volein, N. Everdell, C. E. Elwell, and M. H. Johnson, “Social perception in infancy: A near infrared spectroscopy study,” *Child Dev.*, vol. 80, no. 4, pp. 986–999, 2009, doi: 10.1111/j.1467-8624.2009.01312.x.

[90] S. Lloyd-Fox *et al.*, "Functional near infrared spectroscopy (fNIRS) to assess cognitive function in infants in rural Africa," *Sci. Rep.*, vol. 4, p. 4740, 2014, doi: 10.1038/srep04740.
[91] P. Phan, D. Highton, J. Lai, M. Smith, C. Elwell, and I. Tachtsidis, "Multi-channel multi-distance broadband near- infrared spectroscopy system to measure the spatial response of cellular oxygen metabolism and tissue oxygenation," *Biomed. Opt. Express*, vol. 7, no. 4424, 2016, doi: 10.1364/BOE.7.004424.
[92] B. Molavi and G. A. Dumont, "Wavelet-based motion artifact removal for functional near-infrared spectroscopy," *Physiol. Meas. Physiol. Meas*, vol. 33, no. 33, pp. 259–270, 2012, doi: 10.1088/0967-3334/33/2/259.
[93] A. Duncan *et al.*, "Optical pathlength measurements on adult head, calf and forearm and the head of the newborn infant using phase resolved optical spectroscopy," *Phys. Med. Biol.*, vol. 40, no. 2, p. 295, 1995, [Online]. Available: http://stacks.iop.org/0031-9155/40/i=2/a=007.
[94] J. M. Kilner, J. Mattout, R. Henson, and K. J. Friston, "Hemodynamic correlates of EEG: A heuristic," *Neuroimage*, 2005, doi: 10.1016/j.neuroimage.2005.06.008.
[95] M. J. Rosa, J. Kilner, F. Blankenburg, O. Josephs, and W. Penny, "Estimating the transfer function from neuronal activity to BOLD using simultaneous EEG-fMRI," *Neuroimage*, 2010, doi: 10.1016/j.neuroimage.2009.09.011.
[96] Y. Benjamini and Y. Hochberg, "Controlling the false discovery rate: a practical and powerful approach to multiple testing," *J. R. Stat. Soc. B*, vol. 57, pp. 289–300, 1995, doi: 10.2307/2346101.
[97] K. J. Friston, A. P. Holmes, K. J. Worsley, J.-P. Poline, C. D. Frith, and R. S. J. Frackowiak, "Statistical parametric maps in functional imaging: A general linear approach," *Hum. Brain Mapp.*, vol. 2, no. 4, pp. 189–210, 1994, doi: https://doi.org/10.1002/hbm.460020402.
[98] M. L. Schroeter *et al.*, "Towards a standard analysis for functional near-infrared imaging.," *Neuroimage*, vol. 21, no. 1, pp. 283–290, Jan. 2004, doi: 10.1016/j.neuroimage.2003.09.054.
[99] S. Shimada and K. Hiraki, "Infant's brain responses to live and televised action.," *Neuroimage*, vol. 32, no. 2, pp. 930–939, Aug. 2006, doi: 10.1016/j.neuroimage.2006.03.044.
[100] Y. Minagawa-Kawai, H. van der Lely, F. Ramus, Y. Sato, R. Mazuka, and E. Dupoux, "Optical Brain Imaging Reveals General Auditory and Language-Specific Processing in Early Infant Development," *Cereb. Cortex*, vol. 21, no. 2, pp. 254–261, Feb. 2011, doi: 10.1093/cercor/bhq082.
[101] P. Pinti, M. F. Siddiqui, A. D. Levy, E. J. H. Jones, and I. Tachtsidis, "An analysis framework for the integration of broadband NIRS and EEG to assess neurovascular and neurometabolic coupling," *Sci. Rep.*, vol. 11, no. 1, p. 3977, 2021, doi: 10.1038/s41598-021-83420-9.
[102] D. Arifler, T. Zhu, S. Madaan, and I. Tachtsidis, "Optimal wavelength combinations for near-infrared spectroscopic monitoring of changes in brain tissue hemoglobin and cytochrome c oxidase concentrations," *Biomed. Opt. Express*, 2015, doi: 10.1364/boe.6.000933.
[103] F. Shi *et al.*, "Infant brain atlases from neonates to 1- and 2-year-olds," *PLoS One*, 2011, doi: 10.1371/journal.pone.0018746.
[104] M. Jenkinson, M. Pechaud, and S. Smith, "BET2: MR-based estimation of brain, skull and scalp surfaces," 2005.
[105] S. Brigadoi *et al.*, "Image reconstruction of oxidized cerebral cytochrome C oxidase changes from broadband near-infrared spectroscopy data," *Neurophotonics*, 2017, doi:

10.1117/1.NPh.4.2.021105.
[106] A. Corlu *et al.*, “Diffuse optical tomography with spectral constraints and wavelength optimization,” *Appl. Opt.*, 2005, doi: 10.1364/AO.44.002082.
[107] M. Schweiger and S. Arridge, “The Toast++ software suite for forward and inverse modeling in optical tomography,” *J. Biomed. Opt.*, 2014, doi: 10.1117/1.jbo.19.4.040801.
[108] F. Bevilacqua, D. Piguet, P. Marquet, J. D. Gross, B. J. Tromberg, and C. Depeursinge, “In vivo local determination of tissue optical properties: applications to human brain,” *Appl. Opt.*, 1999, doi: 10.1364/ao.38.004939.
[109] G. Strangman, J. P. Culver, J. H. Thompson, and D. A. Boas, “A quantitative comparison of simultaneous BOLD fMRI and NIRS recordings during functional brain activation,” *Neuroimage*, vol. 17, no. 2, pp. 719–731, 2002, doi: 10.1016/S1053-8119(02)91227-9.
[110] A. Custo, W. M. Wells, A. H. Barnett, E. M. C. Hillman, and D. A. Boas, “Effective scattering coefficient of the cerebral spinal fluid in adult head models for diffuse optical imaging,” *Appl. Opt.*, 2006, doi: 10.1364/AO.45.004747.
[111] J. Zhao, H. S. Ding, X. L. Hou, C. Le Zhou, and B. Chance, “In vivo determination of the optical properties of infant brain using frequency-domain near-infrared spectroscopy,” *J. Biomed. Opt.*, 2005, doi: 10.1117/1.1891345.
[112] H. Bortfeld, E. Wruck, and D. A. Boas, “Assessing infants’ cortical response to speech using near-infrared spectroscopy,” *Neuroimage*, vol. 34, no. 1, pp. 407–415, Jan. 2007, doi: 10.1016/J.NEUROIMAGE.2006.08.010.